NACA RM A51G24

6349

NACA

RESEARCH MEMORANDUM

EXPERIMENTAL AND THEORETICAL STUDY OF THE EFFECTS OF

BODY SIZE ON THE AERODYNAMIC CHARACTERISTICS OF

AN ASPECT RATIO 3.0 WING-BODY COMBINATION

By Edward J. Hopkins and Hubert C. Carel

Ames Aeronautical Laboratory
Moffett Field, Calif.

Classification cancelled (or changed to ...Unclassified)

By ... Nasa Tech Pub Announcement #164

OFFICER AUTHORIZED TO CHANGE)

By...... 3 Aug 56

GRADE OF OFFICER MAKING CHANGE)

5 Apr 61
DATE

NATIONAL ADVISORY COMMITTEE
FOR AERONAUTICS
WASHINGTON
October 4, 1951

319.98/13

TECH LIBRARY KAFB, NM

0142924

NATIONAL ADVISORY COMMITTEE FOR AERONAUTICS

RESEARCH MEMORANDUM

EXPERIMENTAL AND THEORETICAL STUDY OF THE EFFECTS OF

BODY SIZE ON THE AERODYNAMIC CHARACTERISTICS OF

AN ASPECT RATIO 3.0 WING-BODY COMBINATION

By Edward J. Hopkins and Hubert C. Carel

SUMMARY

Measurements were made at a Mach number of 0.25 of the aerodynamic characteristics of a wing having an aspect ratio of 3 combined separately with each of three geometrically similar bodies of revolution, differing only in size, having a fineness ratio of 12.5. The ratios of body diameter to wing span were 0.196, 0.259, and 0.343. The experimental forces and pitching moments are compared with predicted values for the wing, for each of the bodies, for the wing in the presence of each of the bodies, and for the wing-body combinations. Some experimental and calculated results for the wing mounted on a flat-sided body are also included.

Good agreement between the experimental and calculated results was obtained by including the velocities induced by the wing on the body and by the body on the wing in theoretical calculations of the forces and moments on wing-body combinations incorporating relatively large ratios of body diameter to wing span.

INTRODUCTION

The problem of mutual interference between a wing and a body has long been of interest to aircraft designers. This problem has recently become more important with the use of low-aspect-ratio wings to attain efficient high-speed flight because of the relatively large ratios of body diameter to wing span for these combinations. Therefore, a simple but accurate procedure for predicting the forces and moments mutually induced by a wing and a body is of considerable interest.

The investigation reported herein was initiated to ascertain the effect of body size on the low-speed aerodynamic forces and moments of three wing-body combinations and of their components, and to evaluate the adequacy of existing theories for the prediction of these forces and moments. The method of potential flow is used in this report to calculate upwash angles induced by the bodies in the vicinity of the wing. Since the Weissinger method is easily adapted to wings with arbitrary twist distributions and has been shown to give a good representation of the span load distribution (references 1 to 3), the Weissinger method (references 4 and 5) was selected for the calculation of loads induced by the body on the wing. The Multhopp method (reference 6), which takes into account the flow-angle variation along a body induced by the wing-flow field, is applied herein for the prediction of the pitching moments of the bodies in the presence of the wing. The amount of wing load carried over the bodies was calculated by the Lennertz method (reference 7).

NOTATION

C_b bending-moment coefficient $\left[\dfrac{4B}{q\,S_w b} \right.$ or

$$\left. \int_0^1 \left(c_n \frac{c}{c_{av}} \right) \left(\frac{y}{b/2} \right) d\left(\frac{y}{b/2} \right) \right]$$

C_D drag coefficient $\left(\dfrac{drag}{q\,S_w} \right)$

$\left(C_D \right)_{\alpha=0^\circ}$ drag coefficient at an angle of attack of 0°

C_{m_B} pitching-moment coefficient based on body geometry $\left(\dfrac{M}{q\,S_B L} \right)$

C_{m_W} pitching-moment coefficient based on wing geometry $\left(\dfrac{M}{q\,S_w \bar{c}} \right)$

C_{N_B} normal-force coefficient based on body geometry $\left(\dfrac{N}{q\,S_B} \right)$

C_{N_W} normal-force coefficient based on wing

geometry $\left(\dfrac{N}{q\,S_W}\right)$

C_X longitudinal-force coefficient $\left(\dfrac{X}{q\,S_W}\right)$

c_n local normal-force coefficient $\left(\dfrac{\text{local normal force per unit span}}{qc}\right)$

a   distance from body axis

b   wing span

B   bending moment about the body axis

c   local chord

$\bar{c}$ mean aerodynamic chord $\left(\dfrac{\displaystyle\int_{-b/2}^{b/2} c^2\,dy}{\displaystyle\int_{-b/2}^{b/2} c\,dy}\right)$

c_{av} average chord $\left(\dfrac{S_W}{b}\right)$

D   maximum diameter of body or maximum width of body

i_w angle of wing incidence relative to the body axis

L   body length

M   pitching moment about the moment centers shown in figures 1(a) and 1(b)

N   force normal to the body axis and in the vertical plane of symmetry for the bodies and for the wing-body combinations or force normal to the wing-chord plane for the wing alone

q   free-stream dynamic pressure

r   radius of body

r_0 maximum radius of body

S_B maximum cross-section area of body

S_W total wing area

X   force parallel to the body axis

x   longitudinal distance from body nose

y   lateral distance from the vertical plane of symmetry

z   vertical distance from a lateral axis which intersects the body axis

α angle of attack

ϵ upwash angle relative to the free air-stream direction (positive for upwash)

θ angle measured in a plane normal to the body axis from the vertical plane of symmetry below the body axis

MODEL DESCRIPTION

The wing used in the investigation had an aspect ratio of 3, a taper ratio of 0.4, and a hexagonal section 4.5-percent chord thick with rounded ridge lines. (See fig. 1(a).) Each of three geometrically similar bodies of revolution was mounted on this wing with resulting ratios of maximum body diameter to wing span of 0.196, 0.259, and 0.343. As shown in figure 1(b), the wing was in the horizontal plane of symmetry of the bodies of revolution with the 75-percent-chord line of the wing coincident with the midlength point of the bodies. For the tests in which the wing incidence was varied, the wing was rotated about a lateral axis passing through a point at 41.4 percent of the mean aerodynamic chord of the wing. The wing was also combined with a flat-sided body as shown in figure 1(c). Photographs of the wing, of the medium-sized body, and of the wing-body combination are shown in figure 2.

The bodies of revolution had fineness ratios of 12.5 and had contours given by the following equation:

$$r = r_0 \left[1 - \left(1 - \frac{2x}{L} \right)^2 \right]^{3/4} \qquad (1)$$

This body shape has been derived by W. R. Sears and W. Haack and satisfies theoretical criteria for the minimum wave drag at supersonic speeds for a body with a given length and volume. Coordinates for the three bodies of revolution are given in table I. The dimensions of the wing and of the bodies used in reducing the data to coefficient form are presented in table II.

TEST PROCEDURE

The tests were conducted in one of the Ames 7- by 10-foot wind tunnels at a dynamic pressure of 90 pounds per square foot; the Mach number was 0.25; and the Reynolds number was 1.75 million based on the mean aerodynamic chord of the wing. Measurements were made of the normal-force and pitching-moment characteristics of the wing, of the three bodies of revolution, of the wing in the presence of each of the bodies of revolution, and of the wing combined with these bodies. The above aerodynamic characteristics were measured for these wing-body combinations with the wing at an angle of incidence relative to the body axis of 0°, 2°, 4°, 6°, 8°, and 10°. The drag characteristics were measured for the wing, for the bodies, and for the wing-body combinations.

The six-component balance system of the wind tunnel was used to measure the forces and moments for the wing, for the bodies of revolution, and for the wing combined with each of the bodies of revolution. For the measurements of the forces and moments on the wing in the presence of the bodies of revolution, the left wing panel was supported from within the body by a three-component strain-gage system. A gap of about 1/4 inch was required between the wing surface and the body to allow for deflection of the strain gages. To prevent the flow of air through the gap between the wing and the body, a seal consisting of a thin-walled rubber tube filled with air was inserted in the gap. Air pressure in the tube was maintained at a constant value throughout the tests. Calibration of the strain gages with and without the seal indicated a negligible effect of the seal on the calibration. Simultaneous measurements were made of the forces and moments for the wing in the presence of the bodies of revolution by the strain gages and for the wing-body combinations by the wind-tunnel balance system. The forces and moments for the wing in the presence of the flat-sided body were evaluated from a mechanical integration of graphs of the pressure-distribution data.

A rake consisting of five Keil-type yaw tubes was used to measure the flow angles near the large body in the vicinity of the wing. The rake also contained several tubes for measuring the local dynamic pressure. To avoid the zone of influence of the strut, the flow angles were measured in a lateral plane 6.5 inches ahead of the center line of the model support strut, which was located at 0.450L.

CORRECTIONS

The aerodynamic effects due to the presence of the model–support
struts (strut tares) were measured by using an image–strut system.
Strut tares measured in this manner for all angles of attack were applied
to all the data. Image struts for the medium–sized body and wing–body
combination are shown in figures 2(c) and 2(e). As no provision was made
to measure the tares with the wing at angles of incidence other than 0°,
the strut tares for the wing at an angle of incidence of 0° were applied
to the wing–body data for other angles of wing incidence.

No wind–tunnel–wall corrections were applied to the data because the
corrections for wings mounted on large bodies or for large bodies supported
in rectangular wind tunnels have not been calculated. Application of known
wind–tunnel–wall corrections to the data for the wing would have reduced
the slopes of the normal–force and pitching–moment curves about 2 percent.

RESULTS AND DISCUSSION

In the discussion that follows, the experimental results for the
wing, for the bodies, for the wing in the presence of the bodies, and for
the wing–body combinations are presented and compared with the theoretical
results. The detailed procedure used for the application of existing
theories to calculate the normal–force coefficient for the wing–body com-
binations is explained in the appendices.

Wing

The measured normal–force and pitching–moment characteristics of the
wing are shown in figure 3. Shown in the same figure are the results for
the model wing predicted by use of the Weissinger method presented in
reference 4. At small angles of attack the results in figure 3 indicate
that the predicted slopes of the normal–force and pitching–moment curves
are less than the experimental slopes by about 3 and 10 percent, respec-
tively; however, both the experimental slopes would have been reduced by
about 2 percent had the wind–tunnel–wall corrections been applied. Also,
at low angles of attack the predicted aerodynamic center is within 1.5
percent of the mean aerodynamic chord of the experimental aerodynamic
center. The linear theory of Weissinger would not be expected to account
for the rearward movement of the center of pressure because of the sepa-
ration of the air flow from the wing at the higher angles of attack.

Bodies of Revolution

The experimental normal-force and pitching-moment coefficients for the three bodies of revolution are shown in figure 4(a) based on the body geometry and in 4(b) based on the wing geometry. A direct comparison of the experimental pitching-moment results for the three bodies cannot be made in figure 4 because each of the bodies had a different moment center as shown in figure 1(b). However, it was found that with the data of figure 4 referred to the same moment center, the experimental moments for the three bodies were in substantial agreement except for slight differences which may be attributed to inaccuracies in the strut tares, wind-tunnel-wall effects, or model-scale effects.

The characteristics predicted by use of various methods for these bodies are also shown in figure 4. Potential theory (reference 8) results in an overestimate of the pitching moment as indicated in figure 4(a) and gives zero normal force for a closed body. The method of reference 9 is shown to result in excellent correlation with the experimental normal forces but to overestimate the pitching moments. A revised method (reference 10), in which potential theory is considered to apply only over a forward portion of the body, results in the best agreement with the experimental pitching moments but in an underestimation of the normal forces.

Wing in the Presence of the Bodies

A body at an angle of attack induces a flow field which affects the span load distribution of a wing mounted on the body. The upwash angles induced by the body can be calculated from potential-flow considerations by the following equation which is derived in appendix A:

$$\epsilon = -\frac{r^2}{a^2} \; \alpha \cos 2\theta = -r^2 \left[\frac{z^2 - y^2}{(z^2 + y^2)^2} \right] \alpha \qquad (2)$$

The upwash angle given by the above equation is equal to the angle of attack at the intersection of the lateral plane of symmetry and the body surface ($\theta = \pi/2$). To evaluate the adequacy of potential theory for the midwing position, measurements of the upwash angle were made at 41.4 percent of the length of the large body for angles of attack of 4°, 8°, and 12°. As shown in figure 5(a), the upwash angles were predicted with good accuracy except close to the body at the high angles of attack. To ascertain the validity of potential theory for calculating the upwash angles for a wing mounted in higher or lower positions, additional measurements

of the upwash angles were made at an angle of attack of 8°. These results, as shown in figure 5(b), indicate good agreement between the experimental and the theoretical values except for the inner stations at the high positions.

As a first approximation for calculating the induced load, the flow field around the body might be considered independent of the flow field around the wing. Following this assumption, the load induced by the body along the exposed part of the wing span was calculated by the Weissinger method. In the calculations the upwash angles induced by the body were computed from equation (2). In the application of the Weissinger method some discretion was required to handle the discontinuous variation of upwash angle along the wing span ($\epsilon = 0$ across the body). The calculated load on the wing in the presence of the body was considered to consist of the sum of the load induced by the body and that part of the wing-alone load on the exposed part of the wing (reference 4). The details of the procedure used can be found in appendix B. The wing loadings calculated by this procedure for the three wing-body combinations are presented in figure 6. To indicate the amount of the total load theoretically induced by the body, the calculated load for the wing with no body induction is also included in figure 6.

Shown in figure 7(a) are the experimental and calculated normal-force characteristics for the wing mounted separately in the presence of each of the three bodies of revolution (no body forces included in these wing normal forces). The importance of considering the load induced on the wing by the body is indicated in figure 7 by the improved correlation between the experimental and theoretical results.

The bending-moment coefficients for the wing in the presence of each of the bodies are shown in figure 7(b). The agreement between experiment and Weissinger's theory with body induction effects included indicates that the theory provides a reasonable estimate of the spanwise distribution of load. This result is also indicated by the data given in figure 8(a) for the same wing mounted on a relatively flat-sided body. It should be noted that the wing was mounted below the center of the flat-sided body; therefore, the calculated body induction effects are small. (See fig. 5(b).) In the upper part of figure 8(a) are shown the calculated upwash angles for an "equivalent" body of revolution having the same cross-sectional area as the flat-sided body. With the load induced by the body taken into account, the predicted loading coefficients are in excellent agreement with the experimental values as shown in the lower part of figure 8(a). This result is also indicated by the normal-force and bending-moment characteristics (shown in fig. 8(b)) which were calculated from the loading curves for the wing.

Wing Combined With the Bodies of Revolution

For the prediction of the forces and moments of wing–body com-
binations, the effect of the mutual interaction between the wing and the
body should be considered. One important part of this analysis involves
the calculation of the amount of wing load carried over the body. This
problem of load carry–over was first investigated by Dr. Lennertz who con-
sidered an idealized wing–body combination having a spanwise distribution
of circulation to satisfy the condition for minimum induced drag (refer-
ence 7). Dr. Lennertz calculated the simplified case for which the lifting
line and the body axis intersect and a cylindrical body is assumed to
extend to infinity in front of and behind the wing. The results of his
calculations for wing load carry–over as a function of cylinder–diameter
to wing–span ratio are presented in figure 9. To indicate the adequacy
of his simplified theory, the experimental points from the present inves-
tigation are also shown in figure 9. Lennertz's analysis applies to an
infinite cylinder which has no lift at an angle of attack; whereas the
bodies of this investigation had lift at an angle of attack. In order to
eliminate this difference the measurements considered in the comparison
were those for the bodies at 0° and the wing incidence variable. The good
agreement between the predicted values for $i_w=0$ and measured values for
$\alpha=0$ indicates that (1) Lennertz's results for wings combined with infinitely
long cylinders are applicable to wings with nearly elliptic span loadings
combined with long slender bodies, and (2) approximately the same percent-
age of load is carried from a low–aspect–ratio wing onto a body with the
angle–of–incidence constant and the angle–of–attack variable as with the
angle–of–incidence variable and the angle–of–attack constant.

The experimental and theoretical normal–force characteristics for
each of the three wing–body combinations are presented in figure 10(a).
The predicted values in this figure were computed by adding the normal
forces on the body in the presence of the wing to the product of the cal-
culated normal forces for the wing in the presence of the body times the
Lennertz carry–over factor given in figure 9. The details of the procedure
followed for calculating the normal–force coefficients on the wing–body
combinations are given in appendix B. This method gave good agreement with
the experimental normal forces for the wing combined with either of the two
smallest bodies, but slightly overestimated the normal forces for the larg-
est body.

The experimental pitching–moment results for each of the three wing–
body combinations are presented as coefficients based upon the body geom-
etry in figure 10(b) and based upon the wing geometry in figure 10(c).
The estimated pitching–moment characteristics, also presented in fig-
ure 10(b), were calculated by adding the pitching moments given by the
Multhopp method for a body in the presence of a wing to the experimental
pitching moments for the wing. This procedure was followed as no method

is available for calculating the rearward movement of the center of pressure with angle of attack which is characteristic of thin wings. At small angles of attack, the use of the wing pitching moments from the Weissinger method in place of the experimental pitching moments would have given about the same predicted slopes as those presented in figure 10(b). The experimental pitching-moment results for the wing are also included in figure 10(b) to indicate the contribution of the wing to the predicted results. At small angles of attack good agreement is shown between the experimental pitching-moment coefficients and the estimated coefficients for the three wing-body combinations. At the higher angles of attack the predicted values and experimental results tend to deviate, probably because of a difference in the separation of air flow from the wing mounted on the body as compared to the separation from the isolated wing.

To give a further evaluation of the predicted stability characteristics, the aerodynamic-center locations calculated from the slopes at zero angle of attack of the curves in figure 10 are given in figure 11 as a function of the diameter-to-span ratio. As the diameter-to-span ratio increased, the difference between the experimental and theoretical aerodynamic-center locations varied from less than 1 percent of the mean aerodynamic chord for the smallest body to about 9 percent for the largest body.

In figure 12 are shown the measured longitudinal-force and drag characteristics of the wing, of the three bodies of revolution, and of the three wing-body combinations. For the bodies the longitudinal-force coefficient was relatively constant, except above an angle of attack of about 12°, which indicates that the force resulting from an angle-of-attack change was approximately normal to the wing-chord plane. This result is also indicated for the wing and for the large body by the good agreement between the experimental drag coefficients and the predicted drag coefficients. The predicted drag coefficients were computed by adding to the experimental minimum-drag coefficient the product of the experimental normal force and the sine of the angle of atttck.

Effect of Wing Incidence Changes

The effect of changing the wing incidence on the normal-force and pitching-moment characteristics of the wing combined with each of the bodies of revolution is shown in figure 13. One method of predicting the effect of changing the angle of incidence (at an angle of attack of 0°) on the normal-force coefficients for wing-body combinations involves multiplying the normal forces acting on the exposed part of the wing, as predicted by use of the Weissinger theory, by the Lennertz carry-over factor given in figure 9. As shown in figure 13(c), this method is substantiated by the good agreement between the predicted and experimental results.

The effect of a change in the angle of wing incidence on the aero-dynamic characteristics of the wing in the presence of each of the bodies of revolution is shown in figure 14. With the angle of attack 0°, the use of the Weissinger theory again results in good predictions for the normal-force and bending-moment coefficients produced by a change in the angle of incidence as shown in figures 14(d) and 14(e), respectively.

For either of the above cases in which the incidence of the wing was varied with the bodies held at an angle of attack of 0°, the assumption was made that the forces induced on the wing by the body as a result of the wing changing the flow around the body were insignificant. The good agreement between the predicted and the experimental values indicate that the neglect of this secondary induced effect was justified.

CONCLUSIONS

The experimental results obtained at a Mach number of 0.25 for a thin wing of aspect ratio 3.0 combined with each of several bodies to give diameter-to-span ratios from 0.196 to 0.343 have been presented. Comparisons made between the experimental and the predicted results indicated the following:

1. Good agreement between the experimental and the predicted forces and moments was obtained by including the effects of velocities mutually induced by the wing and the body in the theoretical analysis.

2. At an angle of attack of 8° the upwash angles were accurately predicted, by use of potential theory for a circular cylinder, in a verti-cal plane near the midlength of the body except at span stations close to the body at positions well above the body.

3. The normal forces and bending moments on the wing in the presence of the bodies were accurately predicted by adding the forces and moments produced by a change in angle of attack, calculated by the Weissinger method, to the forces and bending moments induced by the body.

4. The normal forces on the wing-body combinations with the wing incidence fixed were accurately predicted by adding the body forces on the part of the body ahead of the wing to the product of forces on the wing in the presence of the body times the Lennertz carry-over factor.

5. The predicted pitching moments for the wing-body combinations were in good agreement with the experimental values at small angles of attack. For these predictions, the pitching moments for the body in the presence of the wing were calculated by the Multhopp method and added

to the experimental wing pitching moments because no method was available for estimating the nonlinear characteristics of the wing pitching-moment curve at the higher angles of attack.

6. The difference between the experimental and predicted location for the aerodynamic center varied from less than 1 percent of the mean aerodynamic chord for the wing combined with the smallest body to about 9 percent for the wing combined with the largest body.

7. For estimating the forces on the wing-body combinations with the body at an angle of attack of $0°$ and the wing-incidence variable, good predictions were obtained by multiplying the forces on the wing in the presence of the body by the Lennertz carry-over factor.

8. The forces and bending moments on the wing in the presence of the bodies as produced by an angle-of-incidence change with the body at an angle of attack of $0°$ were satisfactorily predicted by utilizing the Weissinger method and neglecting any secondary induction effects from the body.

Ames Aeronautical Laboratory,
       National Advisory Committee for Aeronautics,
              Moffett Field, Calif.

APPENDIX A

UPWASH ANGLE INDUCED BY A BODY OF REVOLUTION

The derivation of the equation for calculating the upwash angles around a body of revolution is as follows:

Assume that the flow normal to the body axis is analogous to the flow around a circular cylinder in a perfect fluid with a velocity equal to the free–stream velocity times the sine of the angle of attack $(U=V_0 \sin \alpha)$. Each cross section of the body may then be replaced by a doublet. For a doublet, the velocity components at any point are expressed in the equations given by Glauert (reference 11).

$$u' = -U \left(1 - \frac{r^2}{a^2} \right) \cos \theta \qquad \text{(A1)}$$

$$v' = U \left(1 + \frac{r^2}{a^2} \right) \sin \theta \qquad \text{(A2)}$$

where

u' radial velocity component

v' circumferential velocity component

U free–stream velocity component normal to the body axis
      $(U=V_0 \sin \alpha)$

V_0 free–stream velocity

r radius of body

a,θ polar coordinates

The vertical velocity component, perpendicular to the free–stream velocity, induced by the body is

$$w = \cos \alpha \left(-u' \cos \theta + v' \sin \theta - V_0 \sin \alpha \right) \qquad \text{(A3)}$$

From the relation $\tan \epsilon = w/V_0$ and from the assumption that for small angles $\cos \alpha \cong 1$, $\sin \alpha \cong \alpha$ and $\tan \epsilon \cong \epsilon$, then by substituting equations (A1) and (A2) in equation (A3) the equation for the upwash angle becomes

$$\epsilon = -\frac{r^2}{\alpha^2} \alpha \cos 2\theta \qquad (A4)$$

or in rectangular coordinates

$$\epsilon = -r^2 \left[\frac{z^2 - y^2}{(z^2 + y^2)^2} \right] \alpha \qquad (A5)$$

APPENDIX B

METHODS USED FOR CALCULATING THE NORMAL-FORCE COEFFICIENTS

ON THE WING-BODY COMBINATIONS

The procedure followed for calculating the normal forces acting on the wing-body combinations is as follows:

1. The upwash angles induced by the bodies were calculated from equation (A4) at wing-span stations $y = r$, $y = 0.383(b/2)$, $y = 0.707(b/2)$, $y = 0.924(b/2)$.

2. A special application of the Weissinger method was required to give a close approximation to the load induced by the body from the discontinuous distribution of ϵ shown in the sketch:
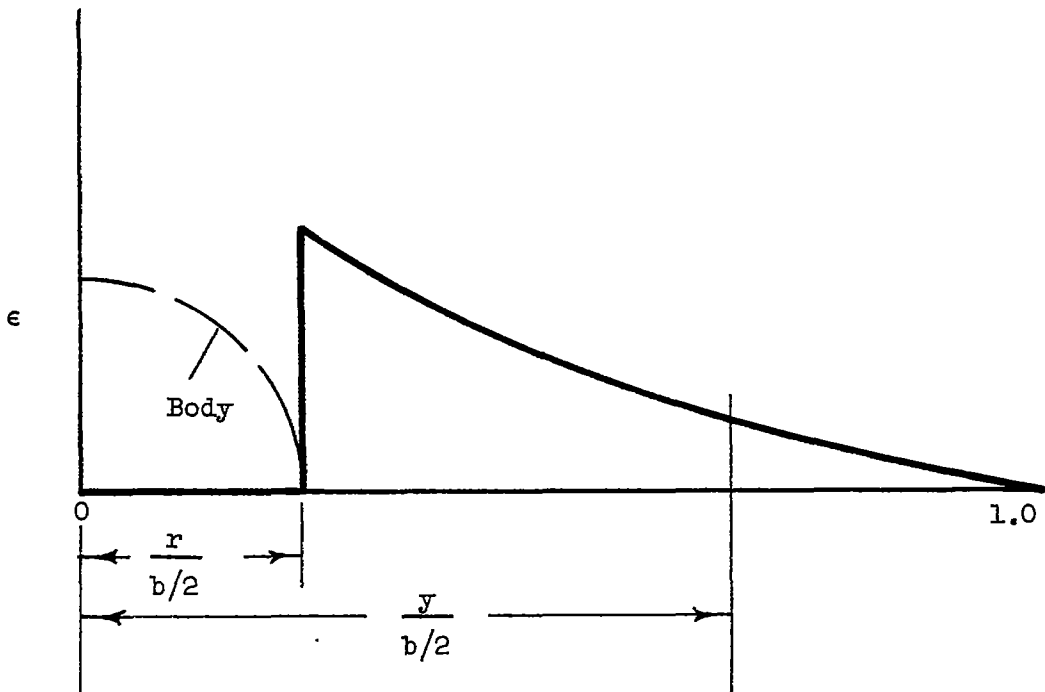
For the first part of the calculation, the upwash angle in the vertical plane of symmetry was assumed to be equal to the computed upwash angle at the wing-body intersection. The dimensionless circulation factors (G_n) were evaluated by solving the following simultaneous equations of the Weissinger method (reference 4):

$$\epsilon_1 = a_{1\ 1}G_1 + a_{1\ 2}G_2 + a_{1\ 3}G_3 + a_{1\ 4}G_4$$

$$\epsilon_2 = a_{2\ 1}G_1 + a_{2\ 2}G_2 + a_{2\ 3}G_3 + a_{2\ 4}G_4$$

$$\epsilon_3 = a_{3\ 1}G_1 + a_{3\ 2}G_2 + a_{3\ 3}G_3 + a_{3\ 4}G_4 \qquad (B1)$$

$$\epsilon_4 = a_{4\ 1}G_1 + a_{4\ 2}G_2 + a_{4\ 3}G_3 + a_{4\ 4}G_4$$

where

ϵ_1 upwash angle at $y = 0.924(b/2)$, radians

ϵ_2 upwash angle at $y = 0.707(b/2)$, radians

ϵ_3 upwash angle at $y = 0.383(b/2)$, radians

ϵ_4 upwash angle at $y = 0$ equal to that at $y = r$

a_{vn} influence coefficient based upon the full-
span geometry (from reference 4)

G_n unknown dimensionless circulation at spanwise station n

Subscript

v,n integers defining specific span station

The loading coefficients were computed from the relation

$$\left(\frac{c_l c}{c_{av}}\right)_n = 2AG_n \qquad (B2)$$

where

A aspect ratio based upon the full wing span and wing area

c_l local lift coefficient

It is necessary to subtract from the above calculated loading coeffi-
cients the portion of these coefficients induced from the assumed distri-
bution of upwash angle over the body ($\epsilon_4 = \epsilon$ at $y = r$). At the suggestion
of Mr. John DeYoung of the Ames Aeronautical Laboratory, the coefficients
to be subtracted were calculated by assuming the portion of the wing
blanketed by the body to be replaced by a 100-percent-chord flap having a
deflection equal to ϵ_4. The flap loading coefficients were obtained by

interpolation from the flap loading curves presented in reference 5. The total loading coefficients induced by the body are shown in the sketch:

For assumed upwash distribution

Total induced by the body

For the inboard flap

$\dfrac{c_l c}{c_{av}}$

Body

0

1.0

$\dfrac{r}{b/2}$ = flap span

$\dfrac{y}{b/2}$
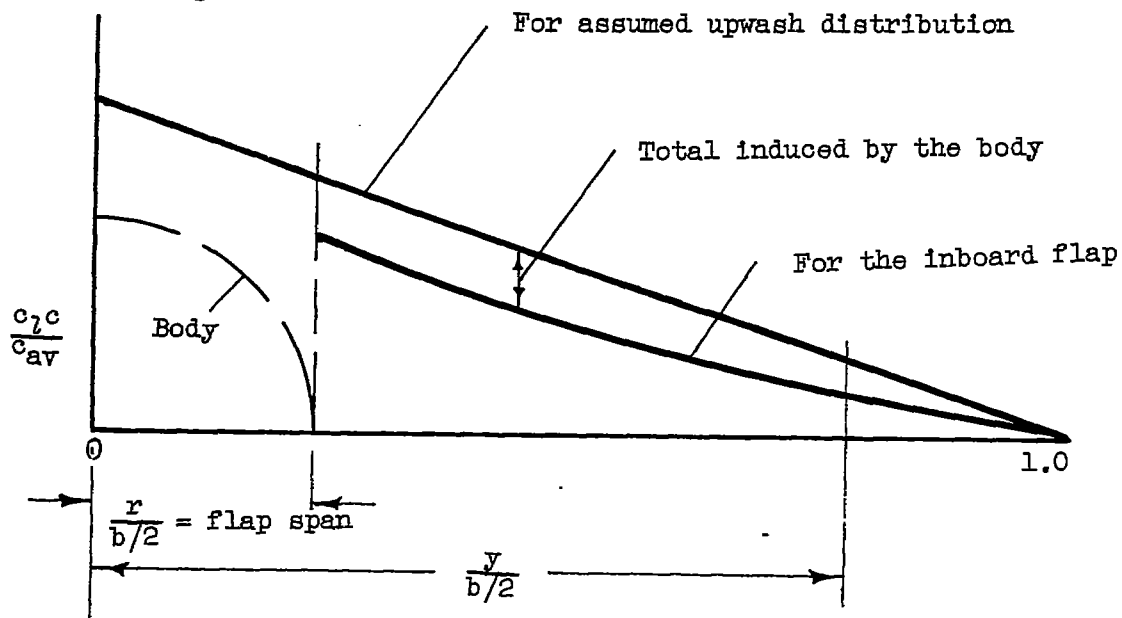
3. The total loading coefficients for the wing in the presence of the body were calculated by adding the total loading coefficient induced by the body on the wing (derived as in paragraph 2) to the loading coefficients for the full-span wing as given in reference 4. This addition is represented in the sketch:

Total acting on the wing in the presence of the body

Total induced by the body

Wing (reference 4)

$\dfrac{c_l c}{c_{av}}$

Body

0   $\dfrac{r}{b/2}$ 1.0

$\dfrac{y}{b/2}$
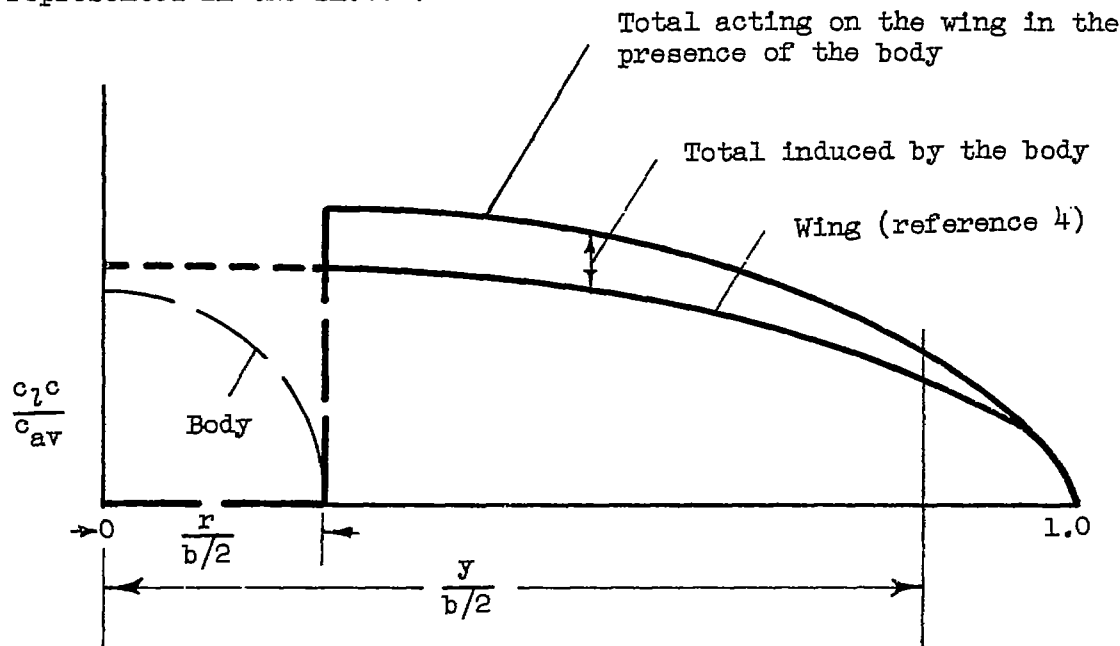
The total normal–force coefficient acting on the wing in the presence of the body was then calculated by the integration:

$$C_N = \frac{1}{\cos \alpha} \int_{\frac{r}{b/2}}^{1.0} \left(\frac{c_l c}{c_{av}} \right)_{\substack{\text{total acting on wing} \\ \text{in presence of body}}} d \left(\frac{y}{b/2} \right) \quad (B3)$$

4. In the calculations for the body in the presence of the wing the normal force of the body behind the wing was assumed to be zero, since the resultant flow is nearly parallel to the body axis. The normal force on the body ahead of the wing, with potential flow assumed, can be shown to be dependent only upon the flow angle at the wing leading edge and the body cross–sectional area at the intersection of the wing leading edge and the body. In reference 6 it is shown that the lift on a body in the presence of a wing is

$$L_B = \int_0^x \frac{dl}{dx} \, dx = 2q\beta S \quad (B4)$$

where

L_B total lift on body from body nose to x

l local lift on body

x longitudinal distance from body nose

S cross–sectional area of body at x

β flow angle $\left(1 + \frac{d\epsilon}{d\alpha} \right)\alpha$

$\dfrac{d\epsilon}{d\alpha}$ rate of change of upwash angle with angle of attack at x from the following equation for an elementary swept horse-shoe vortex assumed to be at the 25–percent–chord line of the wing

$$\frac{d\epsilon}{d\alpha} = \frac{-C_{L\alpha}}{4\pi A} \left\{ \frac{2}{1-\eta^2} + \frac{\sqrt{[\tau - (1-\eta)\tan\Lambda]^2 + (1-\eta)^2}}{\tau(1-\eta)} + \right.$$

$$\frac{\sqrt{[\tau - (1-\eta)\tan\Lambda]^2 + (1+\eta)^2}}{(1+\eta)(\tau + 2\eta\tan\Lambda)} +$$

$$\left. \frac{2\tan\Lambda \sqrt{(\tau + \eta\tan\Lambda)^2 + \eta^2}}{\tau(\tau + 2\eta\tan\Lambda)} \right\} \quad (B5)$$

where

C_{L_α} wing lift—curve slope per radian

η lateral distance $\left(\dfrac{y}{b/2}\right)$ from wing root chord

τ longitudinal distance $\left(\dfrac{x}{b/2}\right)$ from a point on the bound

vortex (x being negative for distances ahead of the bound
vortex)

Therefore for the method used herein, with values of x, β, and S at the
intersection of the wing leading edge and the body surface, it follows
that

$$C_{N_{\substack{\text{body in}\\\text{presence}\\\text{of wing}}}} = \frac{2S_1\beta_1}{S_W \cos \alpha} \tag{B6}$$

where subscript 1 denotes values at the intersection of the wing leading
edge and the body surface.

The normal—force coefficient for the wing—body combination was cal-
culated by adding the normal—force coefficient for the body in the pre-
sence of the wing to the product of the Lennertz carry—over factor times
the normal—force coefficient for the wing in the presence of the body.
This addition is represented as follows:

$$C_{N_W} = \frac{2S_1\beta_1}{S_W \cos \alpha} + \left[\frac{1}{\cos \alpha}\int_{\frac{r}{b/2}}^{1.0}\left(\frac{c_l c}{c_{av}}\right)_{\substack{\text{total acting on wing}\\\text{in presence of body}}} d\left(\frac{y}{b/2}\right)\right]$$

$$\left[\begin{array}{l}\text{Lennertz's carry—over}\\\text{factor, fig. 9}\end{array}\right] \tag{B7}$$

REFERENCES

1. Hunton, Lynn W., and Dew, Joseph K.: The Effects of Camber and Twist on the Aerodynamic Loading and Stalling Characteristics of a Large-Scale 45° Swept-Back Wing. NACA RM A50J24, 1951.

2. Weiberg, James A., and Carel, Hubert C.: Wind-Tunnel Investigation at Low Speed of a Wing Swept Back 63° and Twisted and Cambered for a Uniform Load at a Lift Coefficient of 0.5. NACA RM A50A23, 1950.

3. Hopkins, Edward J.: Lift, Pitching Moment, and Span Load Characteristics of Wings at Low Speed as Affected by Variations of Sweep and Aspect Ratio. NACA TN 2284, 1951.

4. DeYoung, John, and Harper, Charles W.: Theoretical Symmetric Span Loading at Subsonic Speeds for Wings Having Arbitrary Plan Form. NACA Rep. 921, 1948. (Formerly NACA TN's 1476, 1491, and 1772)

5. DeYoung, John: Theoretical Symmetric Span Loading Due to Flap Deflection for Wings of Arbitrary Plan Form at Subsonic Speeds. NACA TN 2278, 1951.

6. Multhopp, H.: Aerodynamics of the Fuselage. NACA TM 1036, 1942.

7. Durand, William Frederick: Aerodynamic Theory. Vol. IV, J. Springer, Berlin, 1934, pp. 152-157.

8. Munk, Max M.: The Aerodynamic Forces on Airship Hulls. NACA Rep. 184, 1924.

9. Allen, H. Julian: Estimation of the Forces and Moments Acting on Inclined Bodies of Revolution of High Fineness Ratio. NACA RM A9I26, 1949.

10. Hopkins, Edward J.: A Semiempirical Method for Calculating the Pitching Moment of Bodies of Revolution at Low Mach Numbers. NACA RM A51C14, 1951.

11. Glauert, H.: The Elements of Aerofoil and Airscrew Theory, Cambridge, England, The University Press, 1943, p. 30.

CONFIDENTIAL

TABLE I

COORDINATES FOR THE BODIES OF REVOLUTION[1]

$\frac{x}{L}$	Small-body radii (in.)	Medium-body radii (in.)	Large-body radii (in.)
0	0	0	0
.025	.72	.95	1.26
.050	1.18	1.57	2.07
.075	1.57	2.08	2.75
.100	1.91	2.53	3.42
.150	2.48	3.28	4.34
.200	2.94	3.89	5.15
.250	3.31	4.38	5.80
.300	3.61	4.77	6.31
.350	3.83	5.07	6.71
.400	3.99	5.28	6.98
.450	4.08	5.40	7.14
.500	4.11	5.44	7.20

[1]Each body is symmetrical about a plane perpendicular to the axis at 0.5L.

TABLE II

DIMENSIONS OF THE WING AND OF THE BODIES

Model	S_w or S_B (sq ft)	$\bar{c}$ or L (ft)
Wing	4.091	1.24
Small body	.369	8.57
Medium body	.646	11.33
Large body	1.132	14.99
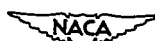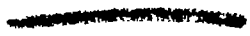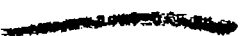
NACA

CONFIDENTIAL

Note: All dimensions in inches.

Leading edge

23°

Moment center

$\bar{c}$ = 14.86

0.414$\bar{c}$

20.00

5.00

0.75 chord line

9.07

21.04

8.00

Rounded ridges

0.300c

0.045c

0.400c

c

0.300c
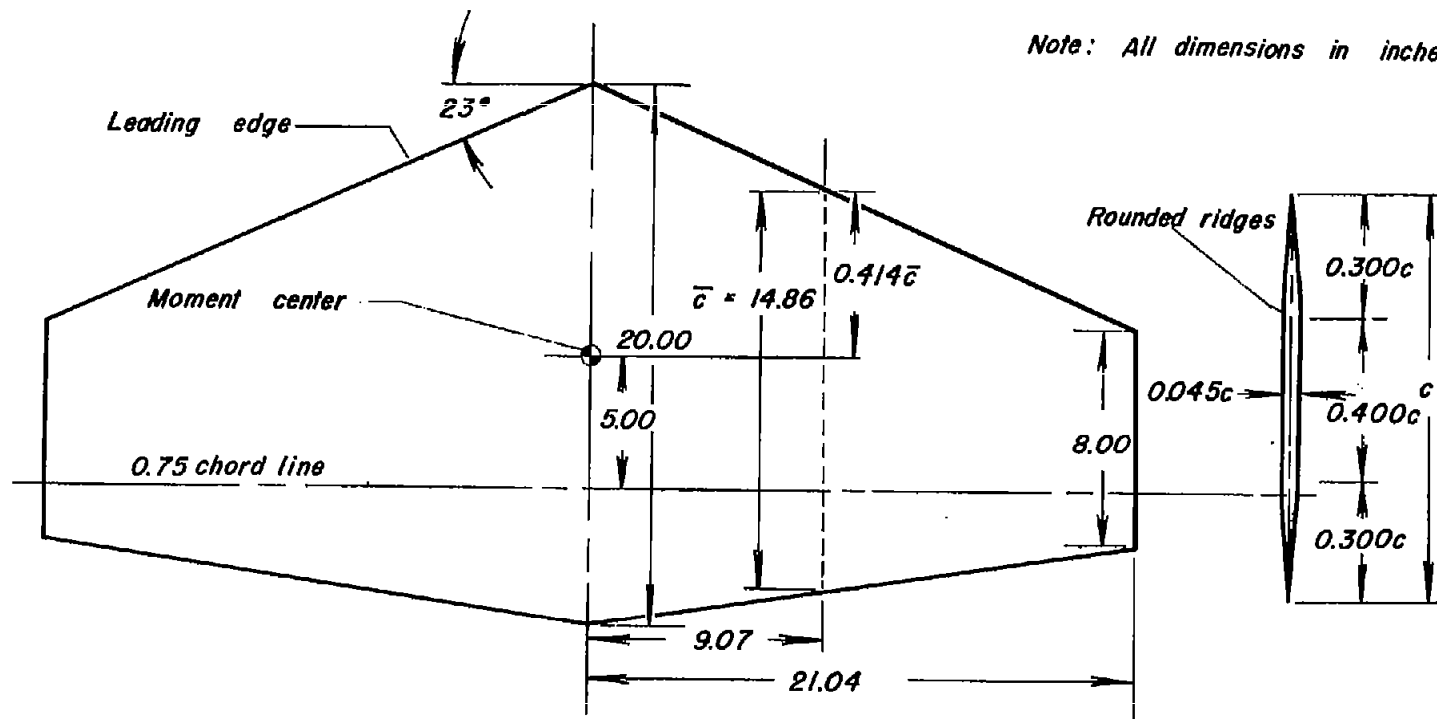
(a)   Wing.

Figure 1.- Dimensions of models.

0.75c

Moment center at 0.414c̄

5"

L = 102.8"
D = 8.2"

D/b = 0.196

5"

L = 136.0"
D = 10.9"

D/b = 0.259

b

D

5"

L = 179.9"
D = 14.4"

D/b = 0.343
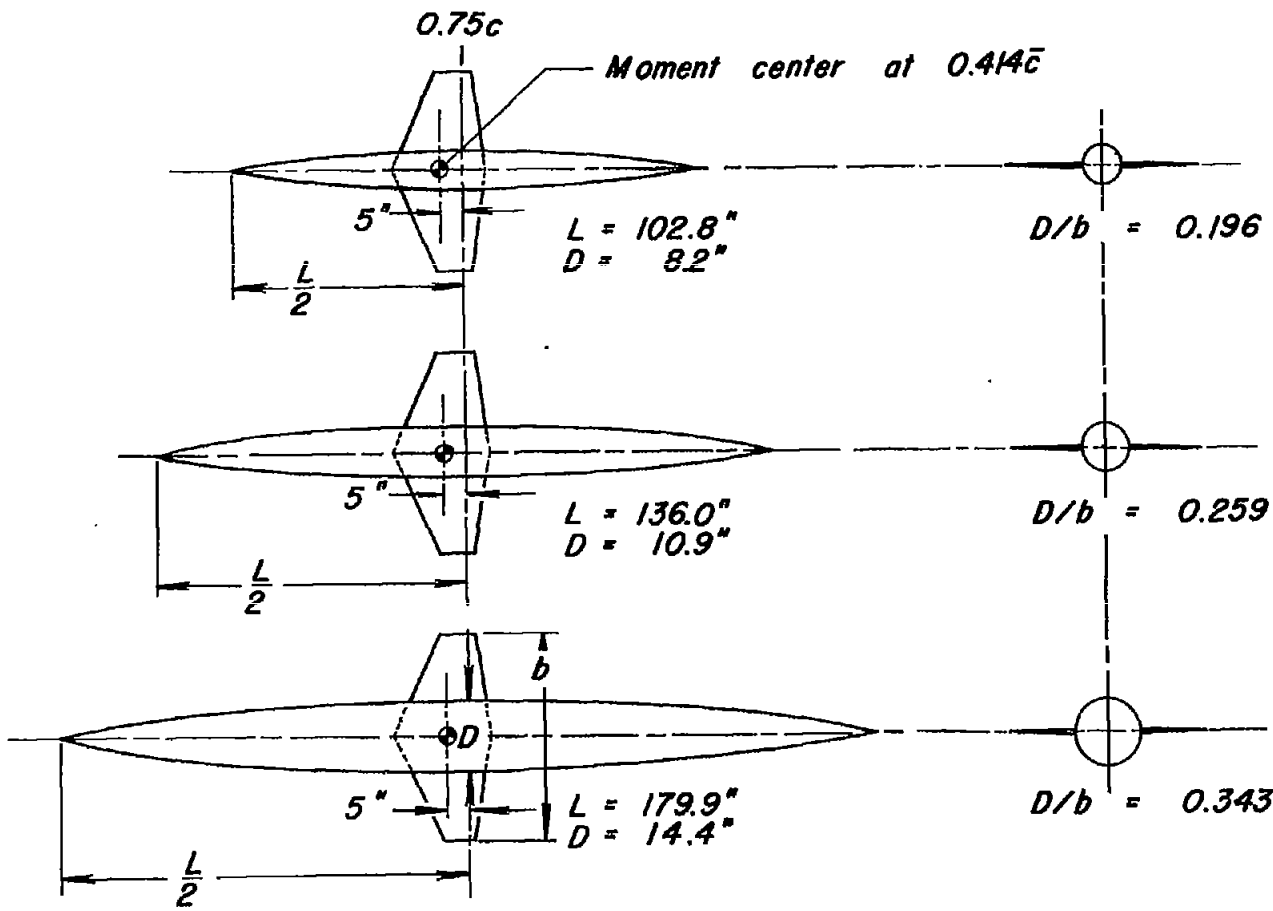
(b)   Wing with bodies of revolution.

Figure 1.— Continued.

0.750c

D/b = 0.250

D

L

0.646L

0.063c̅
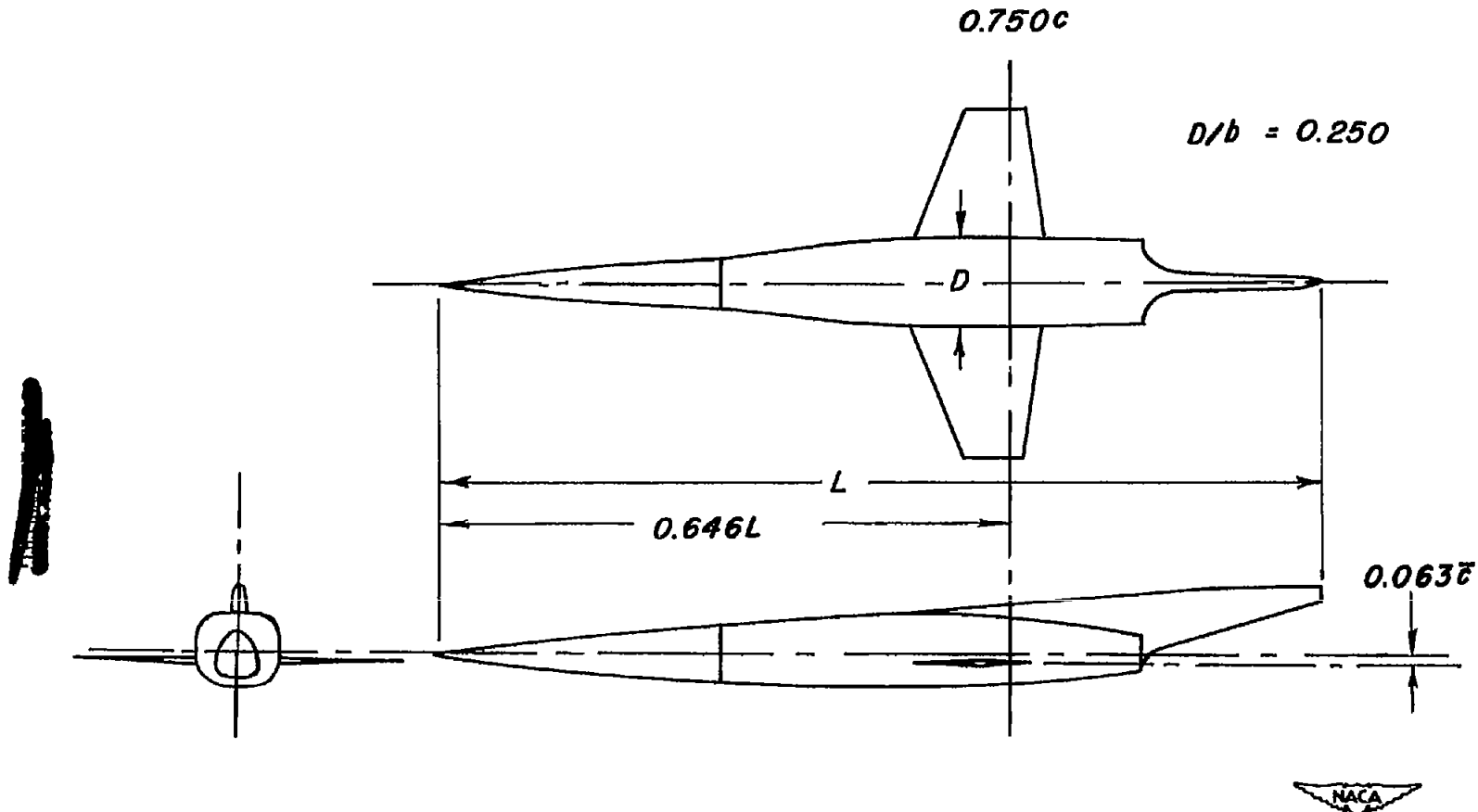
(c)   Wing   with   flat-sided   body.

Figure   1 .- Concluded.

(a) Wing.

Figure 2.— The wing, the medium—sized body of revolution, and
the wing—body combination mounted in one of the Ames
7— by 10—foot wind tunnels.

(b) Body on one strut.

(c) Body with image strut.

Figure 2.— Continued.

(d) Wing—body combination on one strut.

(e) Wing—body combination with image strut.

Figure 2.— Concluded.
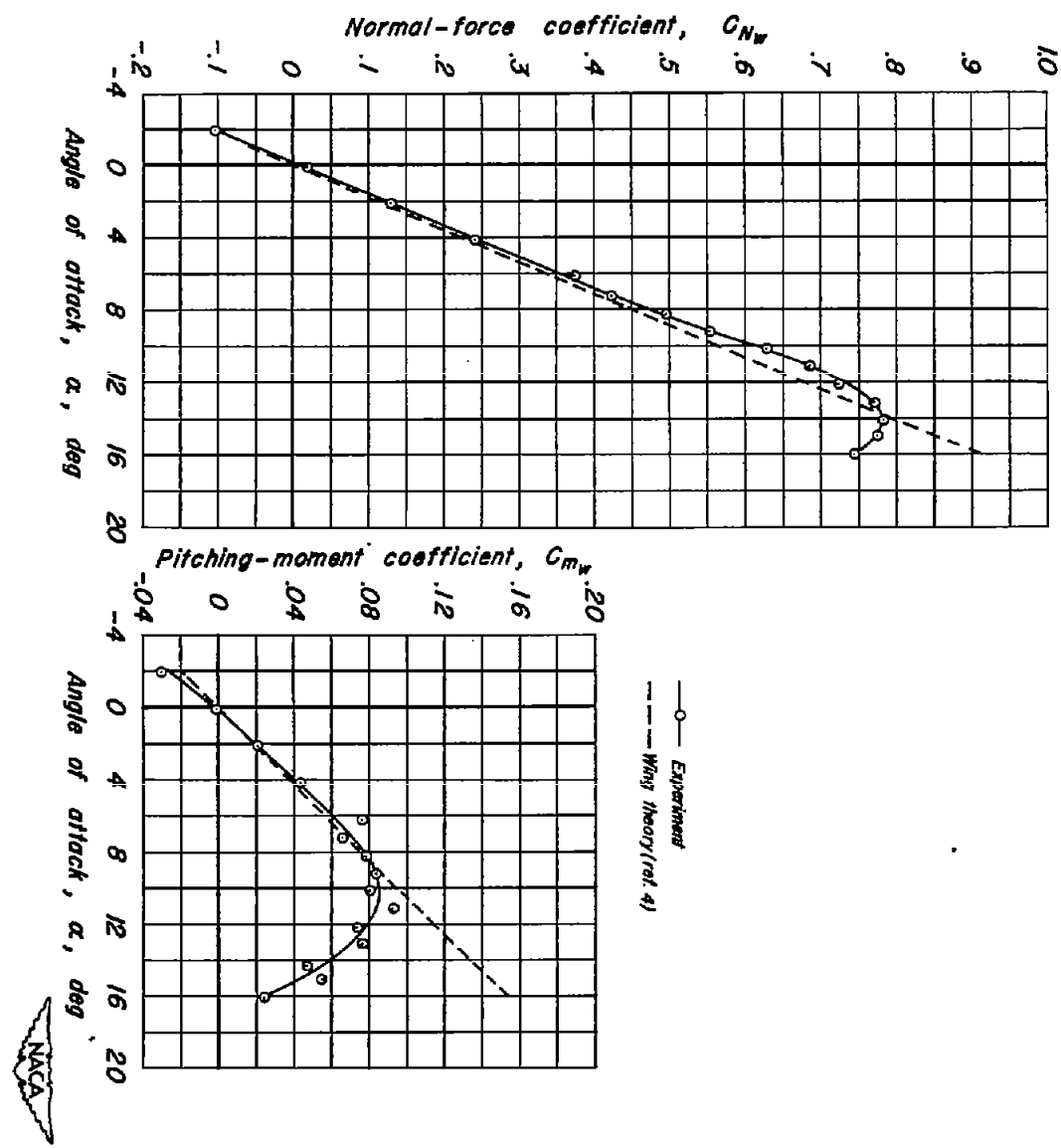
Figure 3.- Comparison between experimental and theoretical aerodynamic characteristics of the wing.
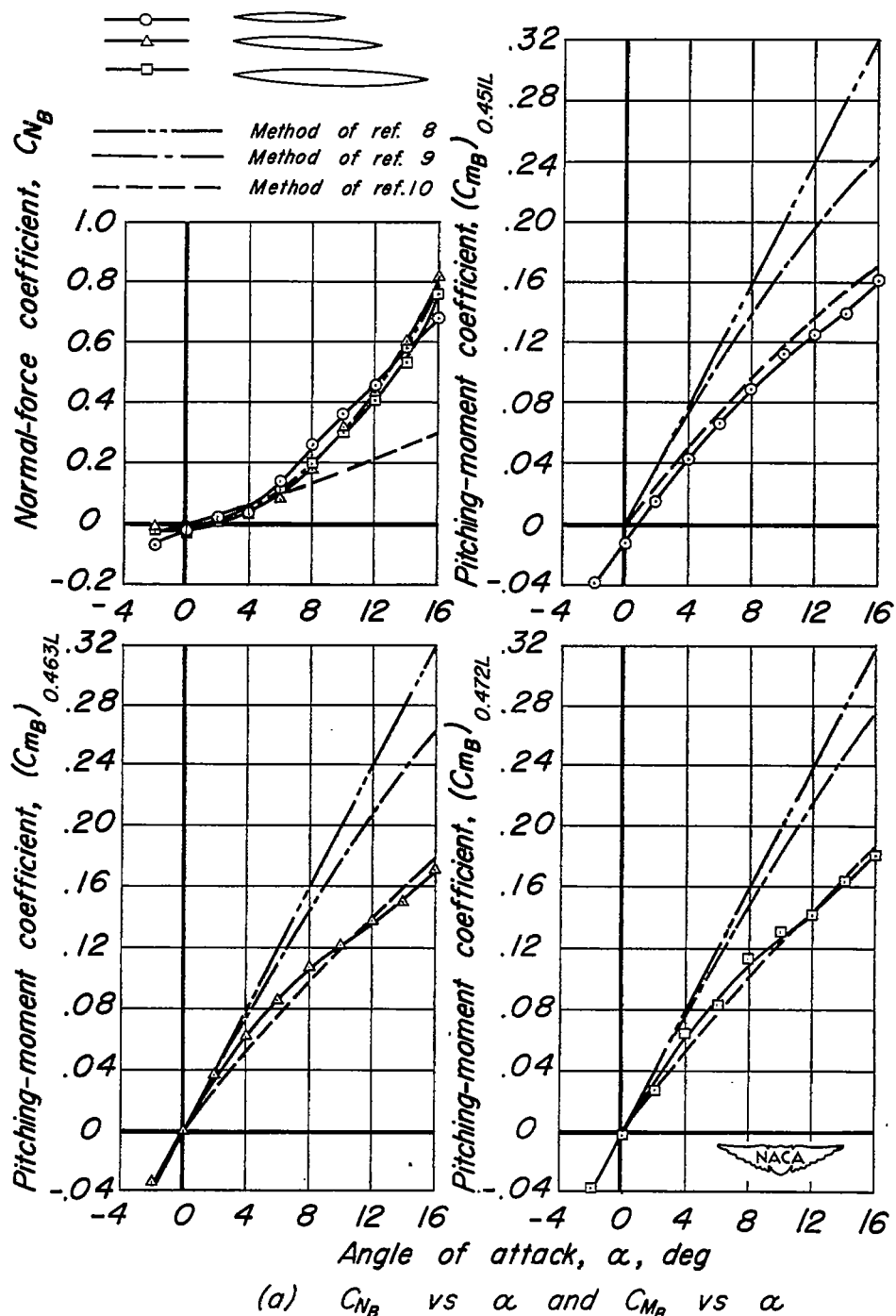
(a)　C_{N_B}　vs　α　and　C_{M_B}　vs　α

Figure 4.— Comparison between experimental and theoretical aerodynamic characteristics of the three bodies of revolution.

Symbols   Experiment
——·—— Method of reference 9
—— ·· —— Method of reference 10

Note: Moment centers are identical to those in figure 4 (a).

(b) C_{N_W} vs α and C_{M_W} vs α.
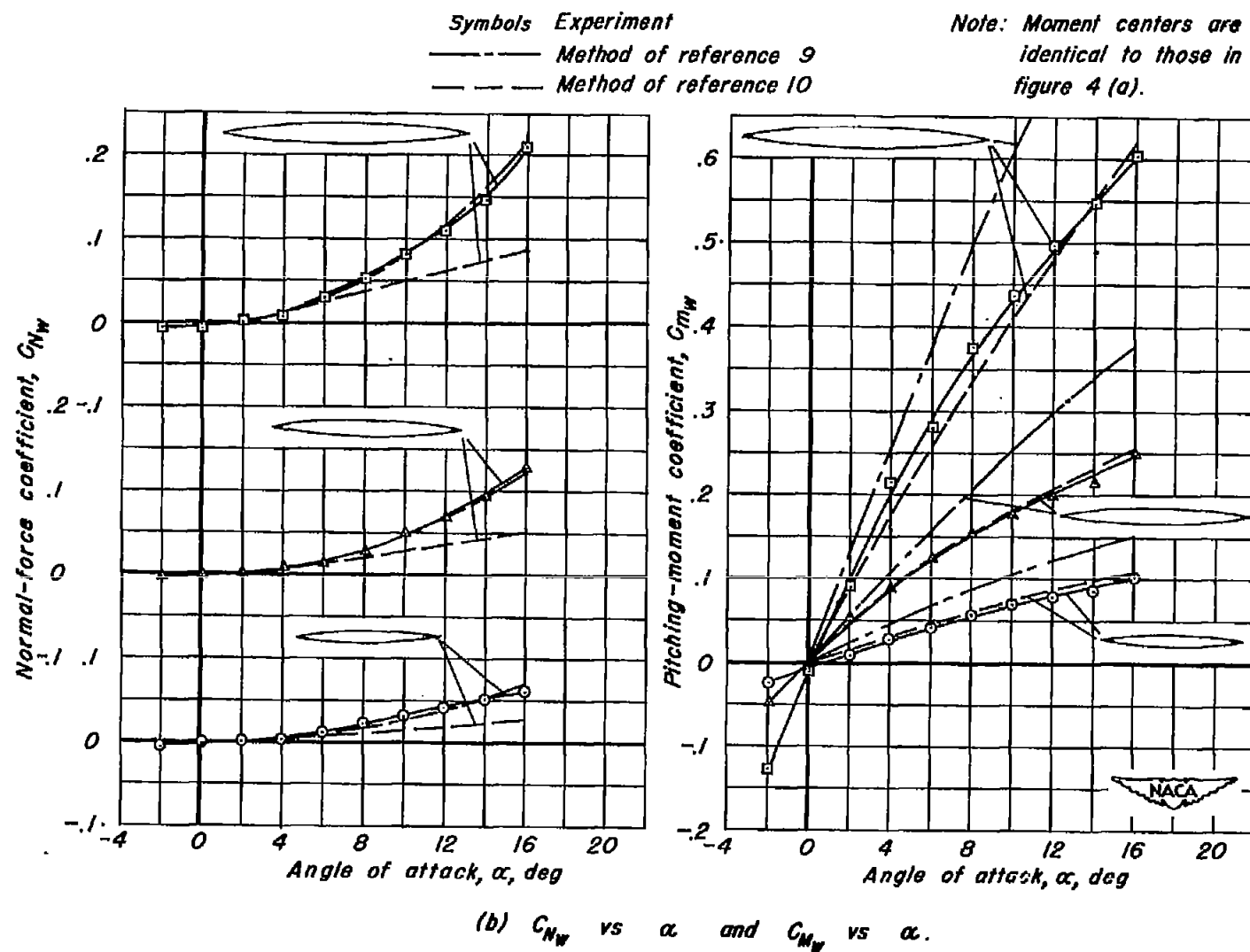
Figure 4.- Concluded.
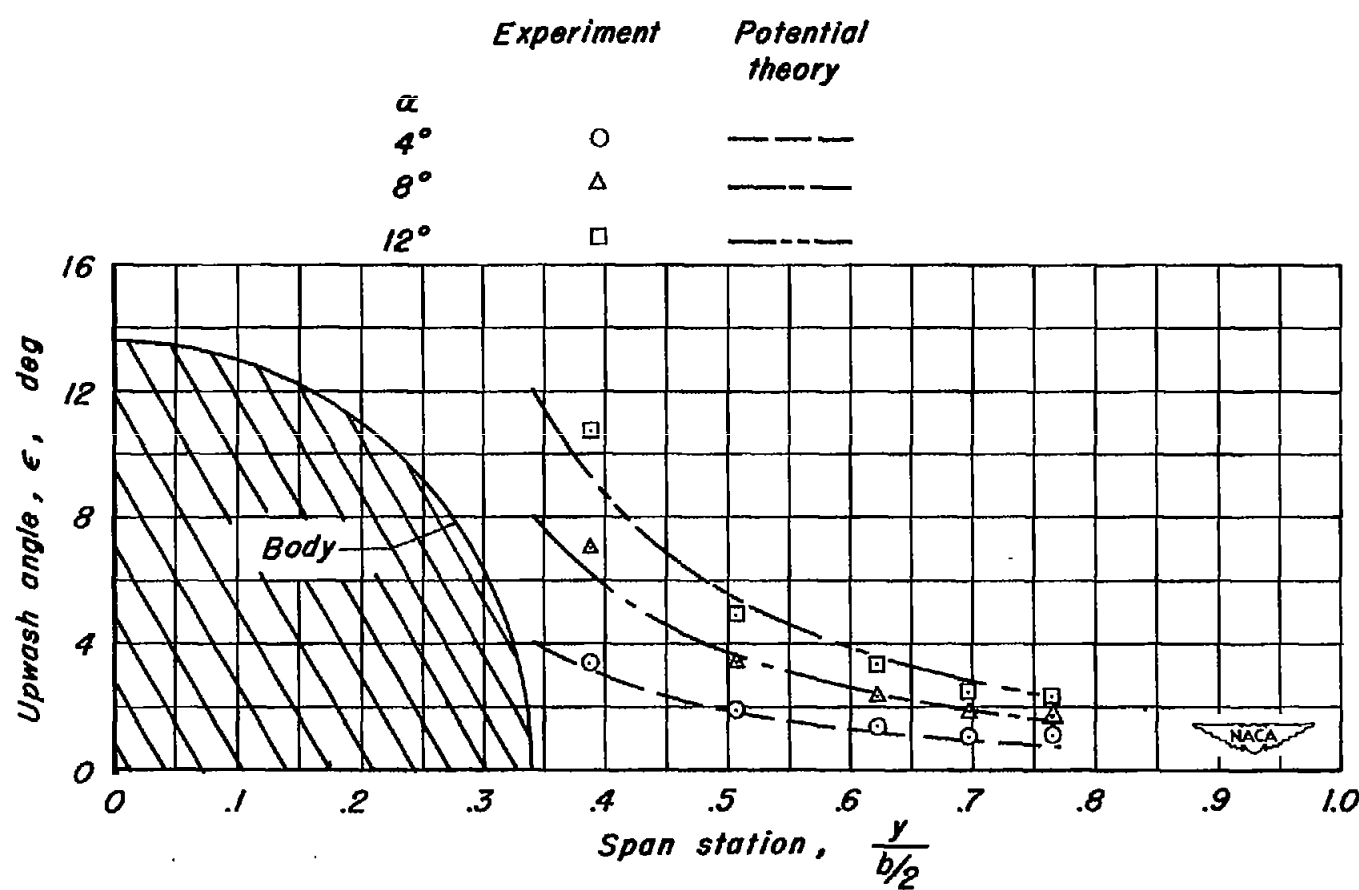
(a) ϵ vs $\frac{y}{b/2}$ in horizontal plane of symmetry.

Figure 5.- Comparison between experimental and theoretical spanwise variation of upwash angles for the large body of revolution. (x = 0.414L).
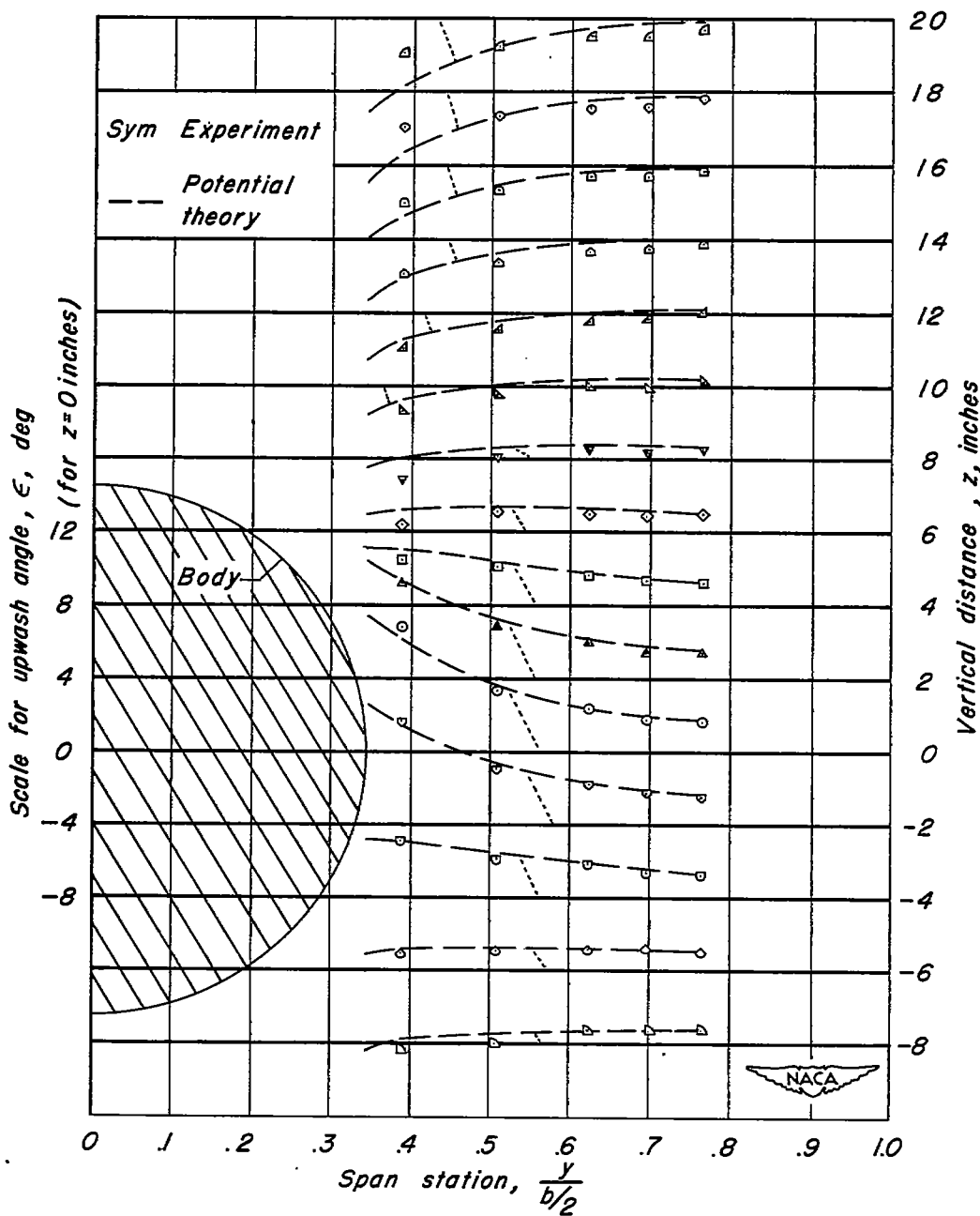
(b) ϵ vs $\frac{y}{b/2}$ for various vertical distances above a lateral line perpendicular to the body axis $(\alpha = 8°)$.

Figure 5.- Concluded.
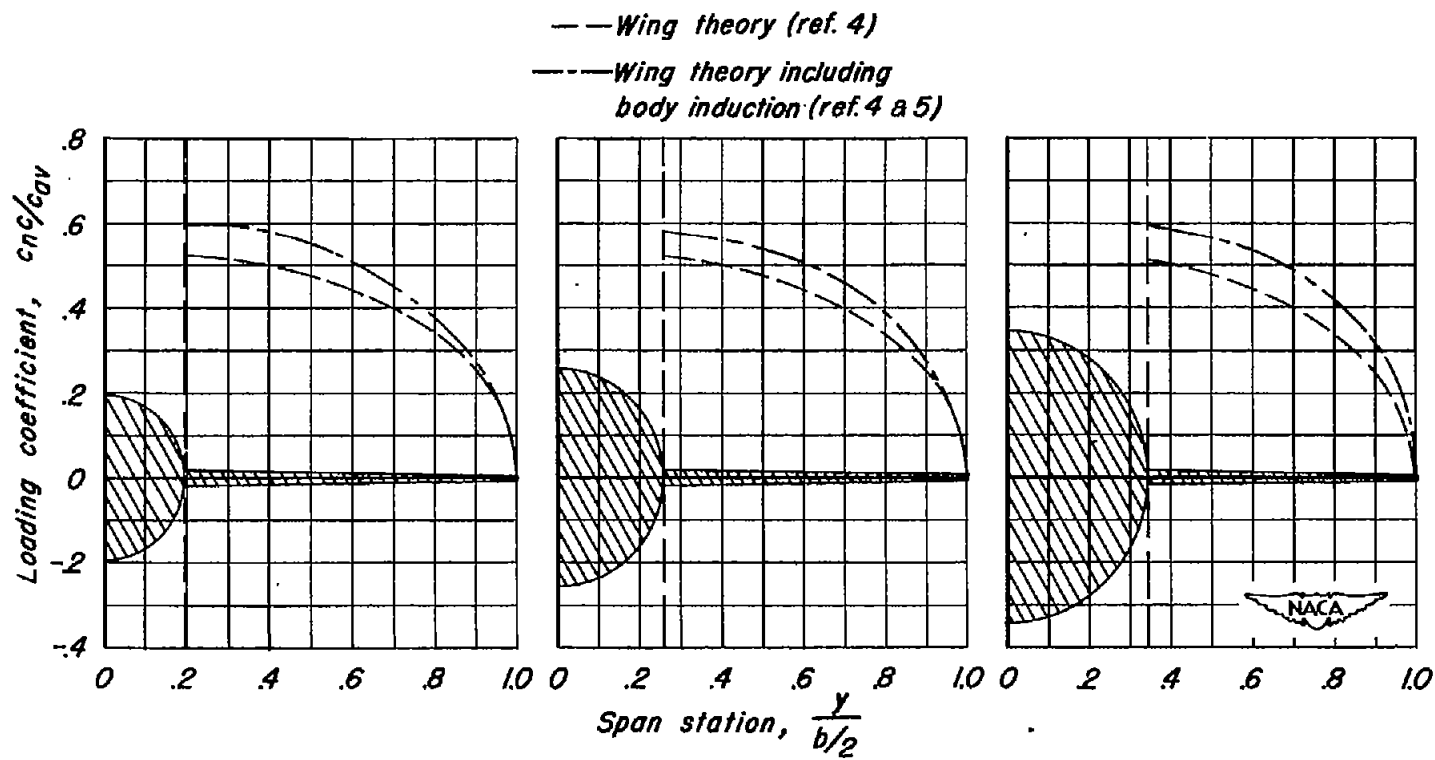
Figure 6.-Theoretical span load distribution for the wing in the presence of the three bodies of revolution. (α = 8°).
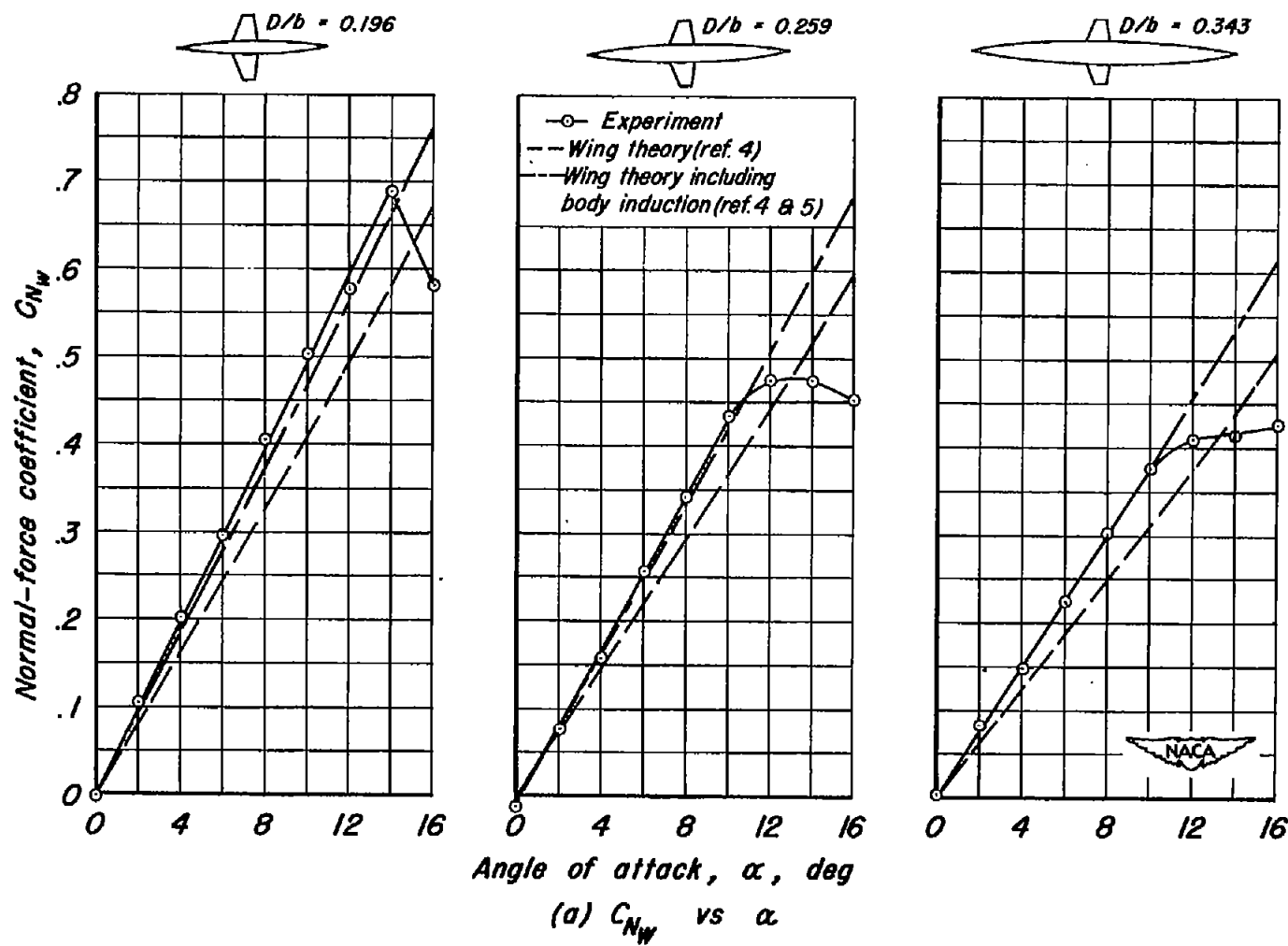
Figure 7.- Comparison between experimental and theoretical aerodynamic characteristics of the wing in the presence of the bodies of revolution.

Bending-moment coefficient, C_b

Angle of attack, α, deg

$D/b = 0.196$

$D/b = 0.259$

$D/b = 0.343$

—○— Experiment
— — Wing theory (ref. 4)
— ·— Wing theory including body induction (ref. 4 & 5)

(b) C_b vs α
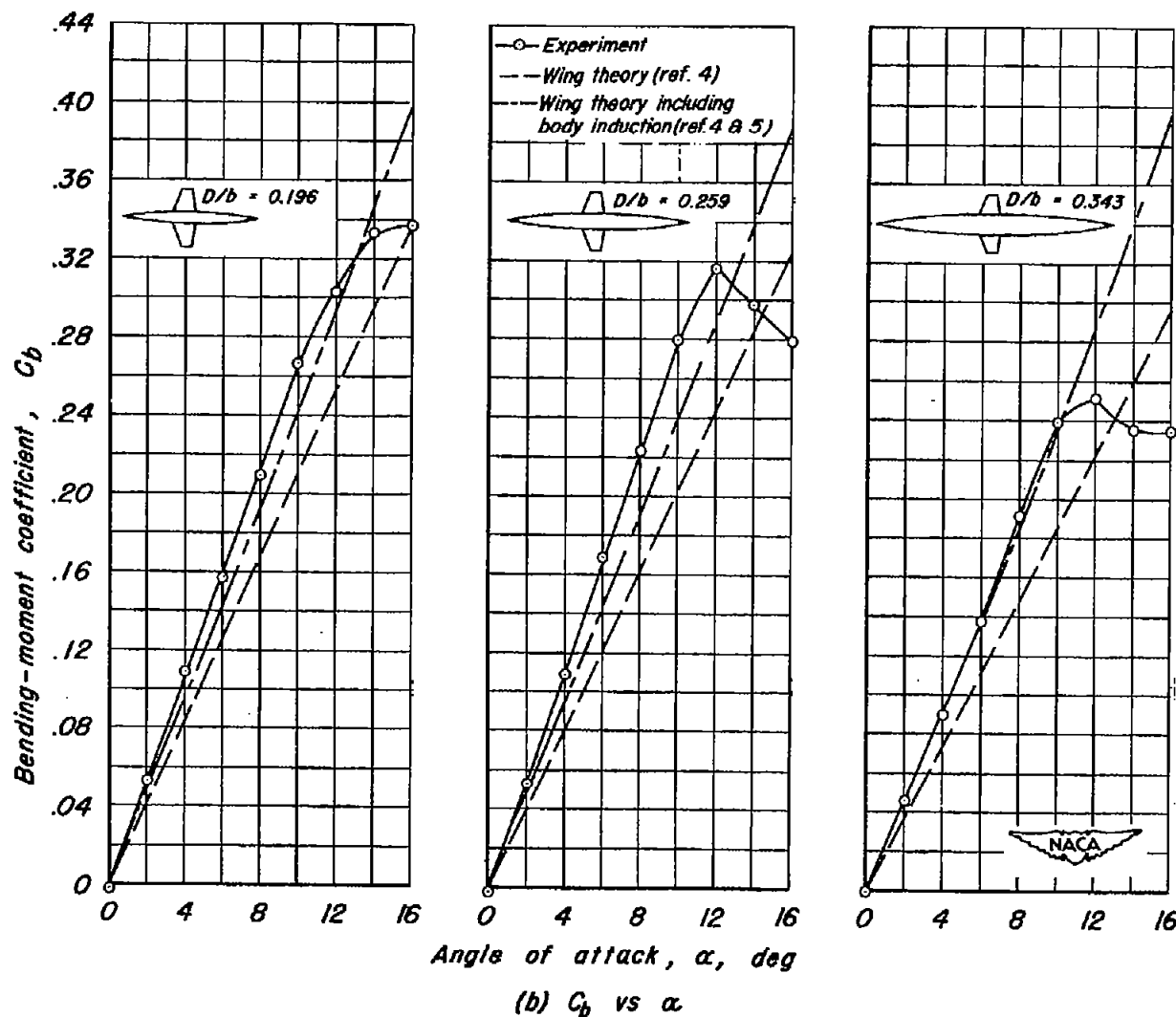
Figure 7.- Concluded.

$(a) \bar{\epsilon}$ vs $\dfrac{y}{b/2}$ and $c_n c/c_{av}$ vs $\dfrac{y}{b/2}$
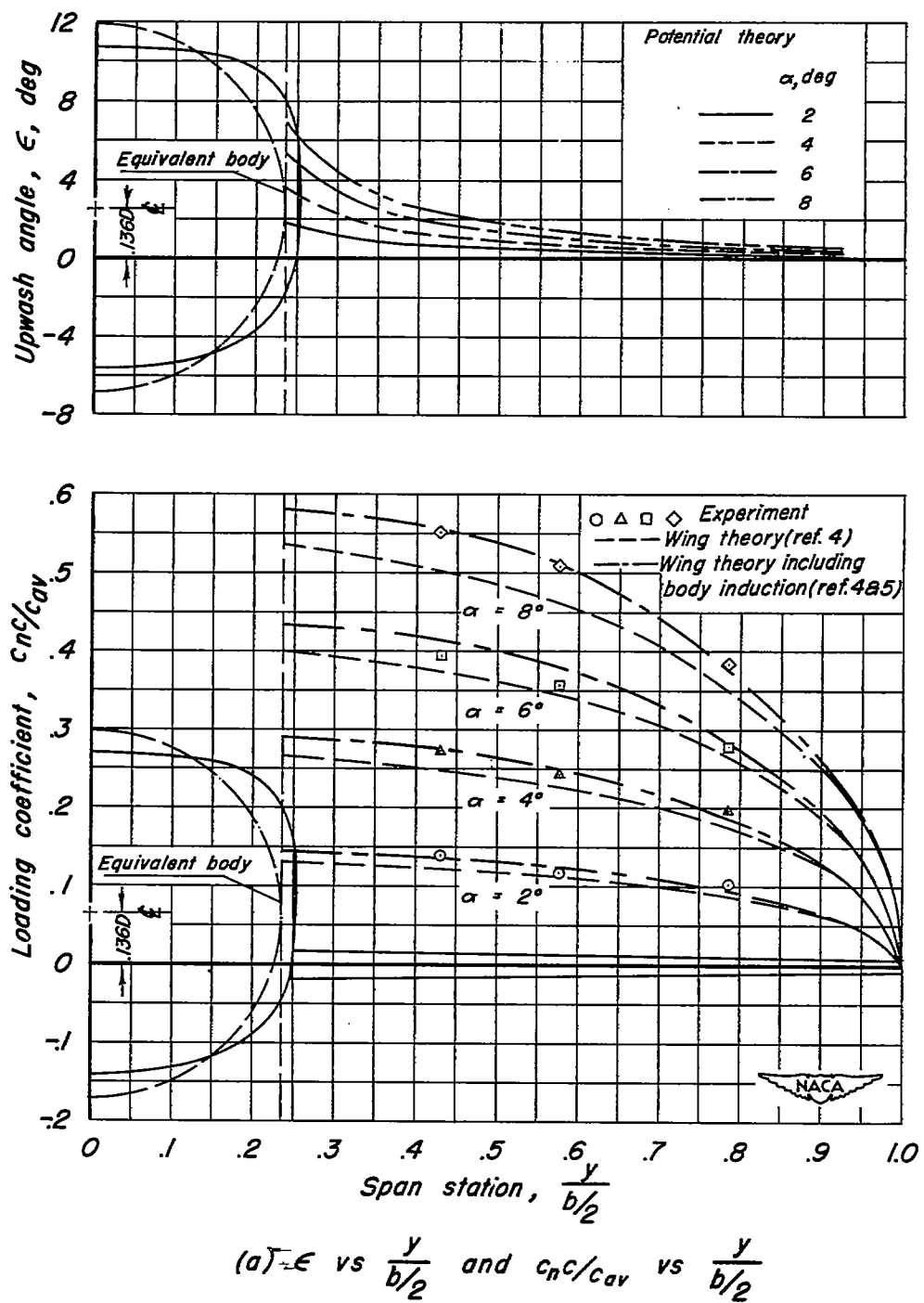
Figure 8.- Experimental and theoretical characteristics for the wing in the presence of the flat-sided body.

(b) C_{N_W} vs α and C_b vs α

Figure 8.- Concluded.

⊙ *Experiment*　　　　　　　　　　—— *Lennertz's theory*

$$\left[\frac{\left(dC_N / di_w \right)_{wing \, + \, body}}{\left(dC_N / di_w \right)_{wing \, in \, presence \, of \, body}} \right]_{\alpha \, = \, 0°} \qquad \left[\frac{\left(dC_N / d\alpha \right)_{wing \, + \, infinite \atop cylinder}}{\left(dC_N / d\alpha \right)_{wing \, in \, presence \, of \atop infinite \, cylinder}} \right]_{i_w = 0°}$$
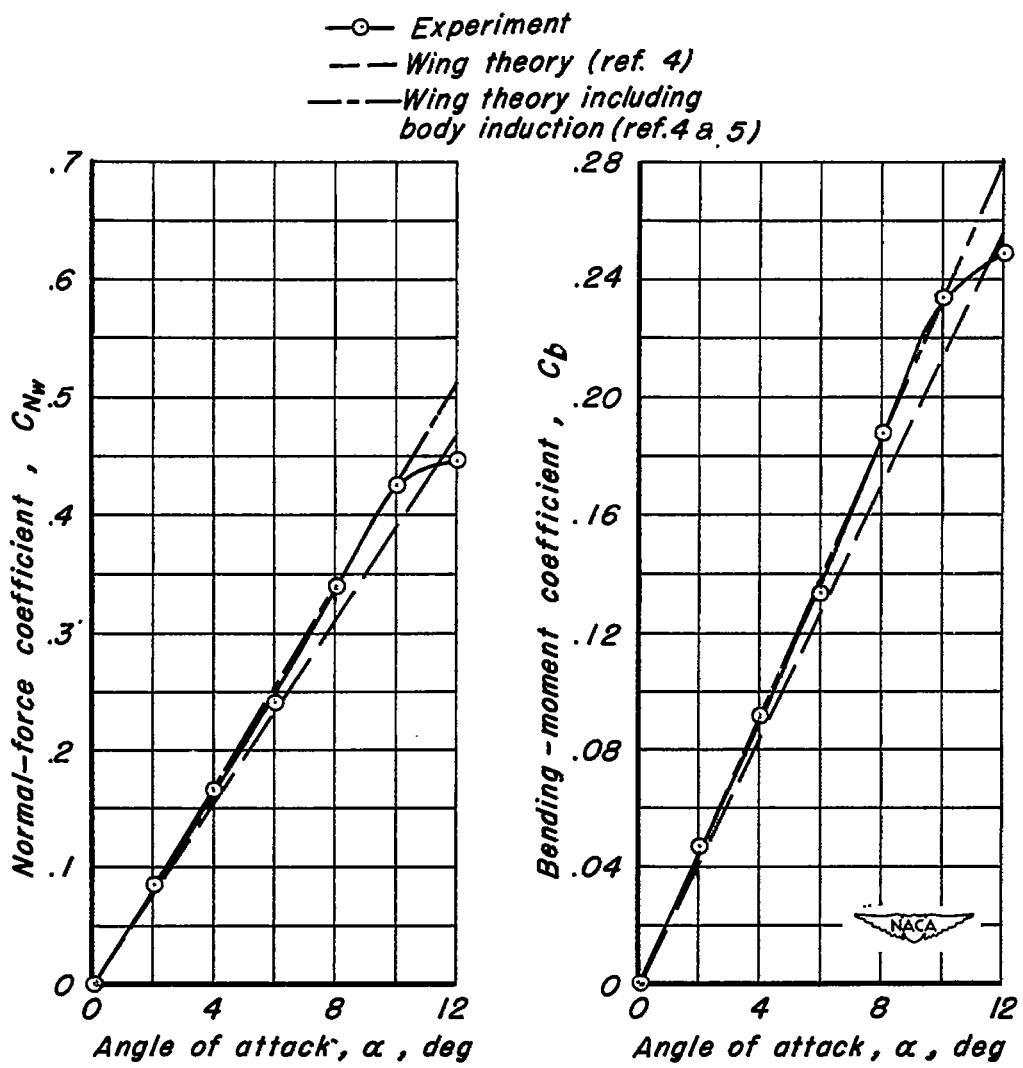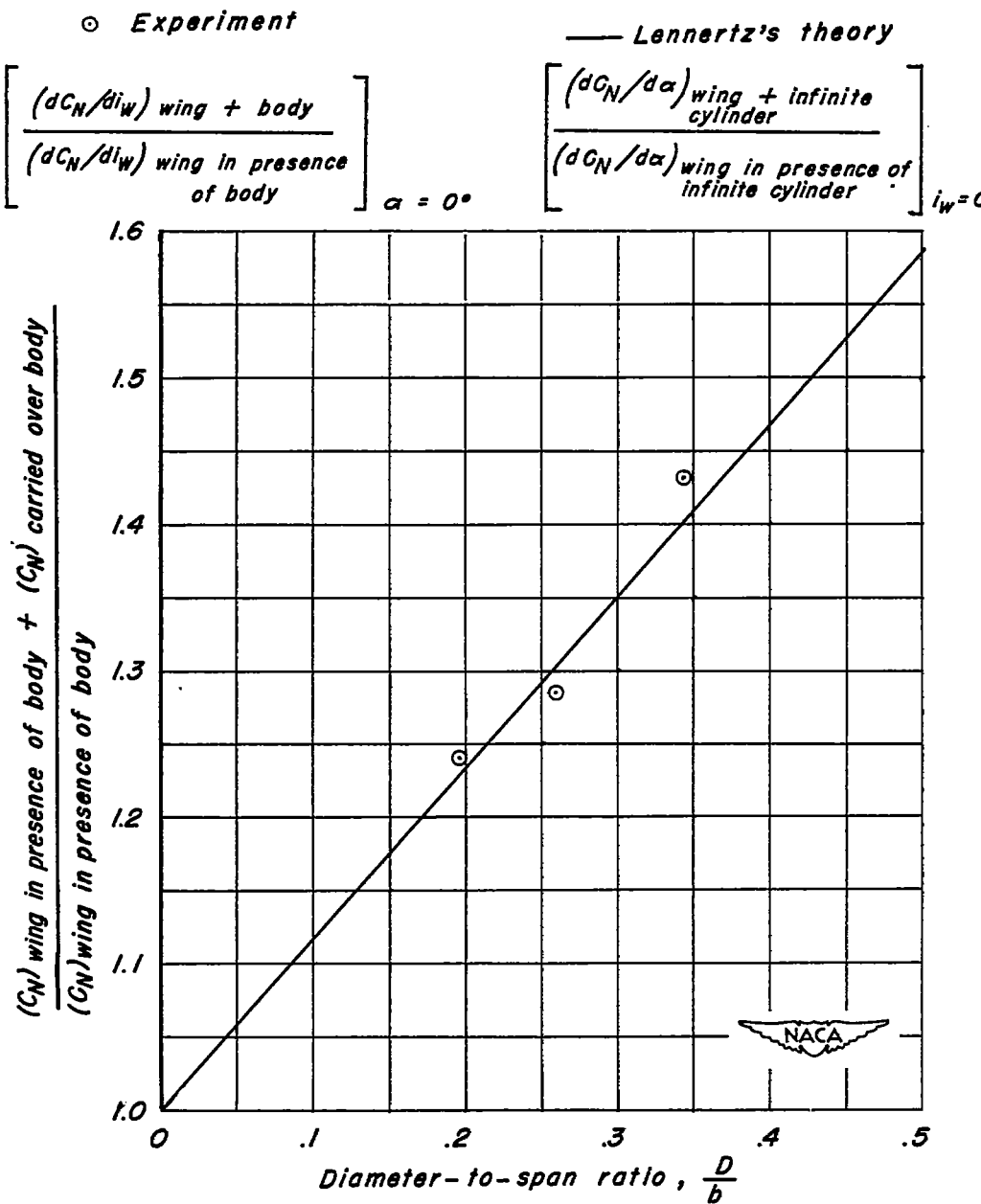
Figure 9.- Effect of body size on the amount of wing normal-force
coefficient carried over bodies of revolution.
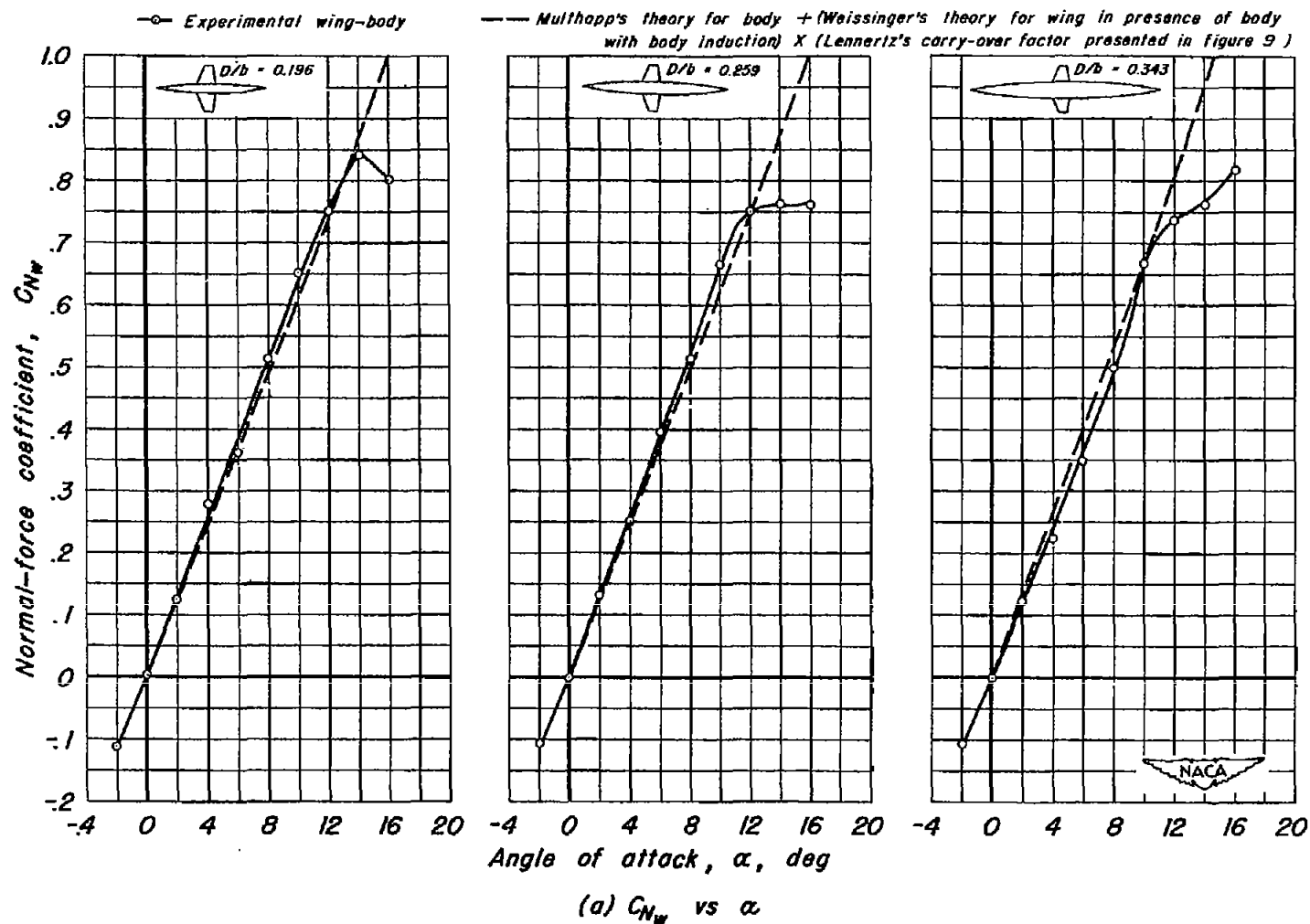
(a) C_{N_W} vs α

Figure 10.- Comparison between experimental and theoretical aerodynamic characteristics of the wing-body combinations.
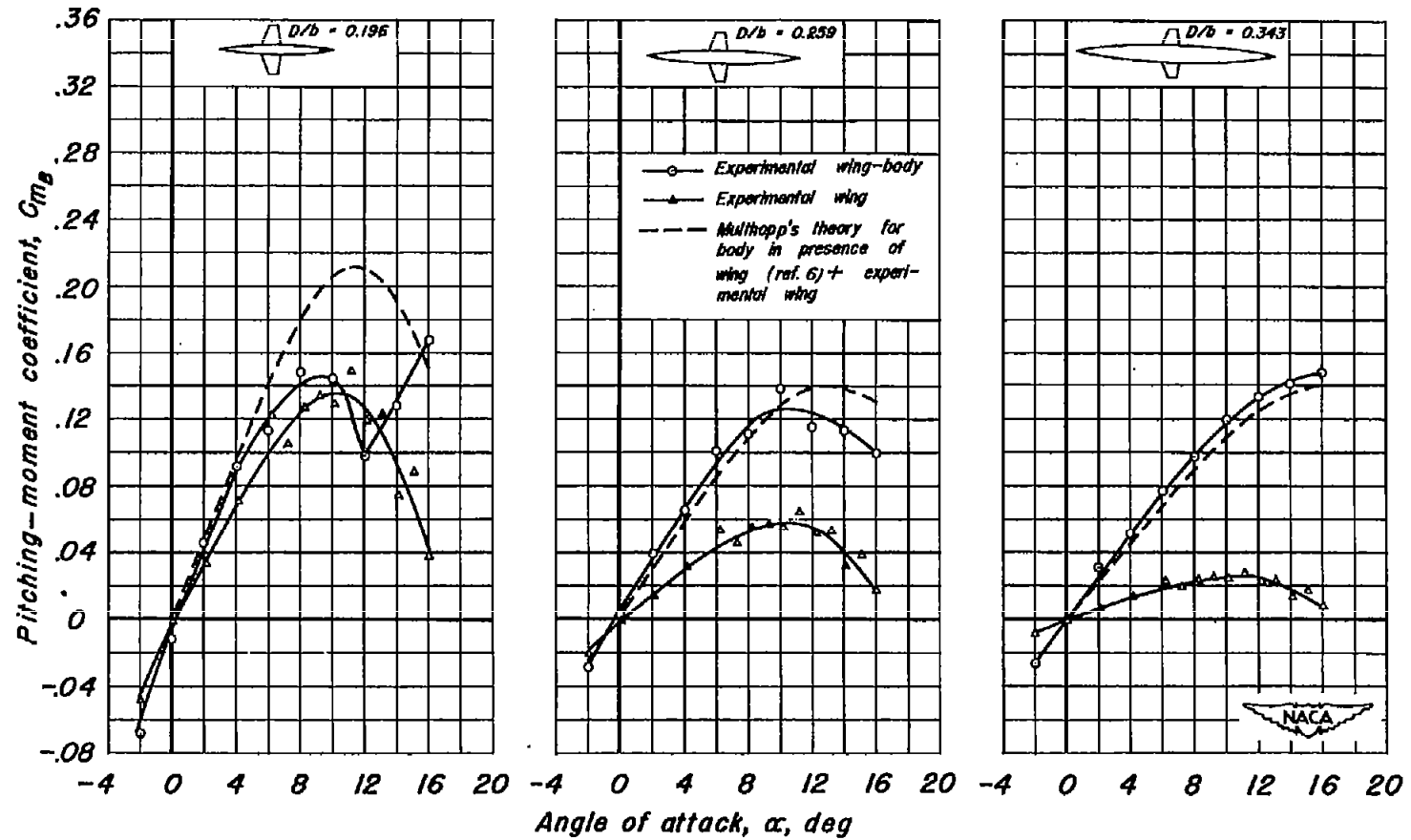
(b) C_{m_B} vs α

Figure 10.- Continued.

CONFIDENTIAL
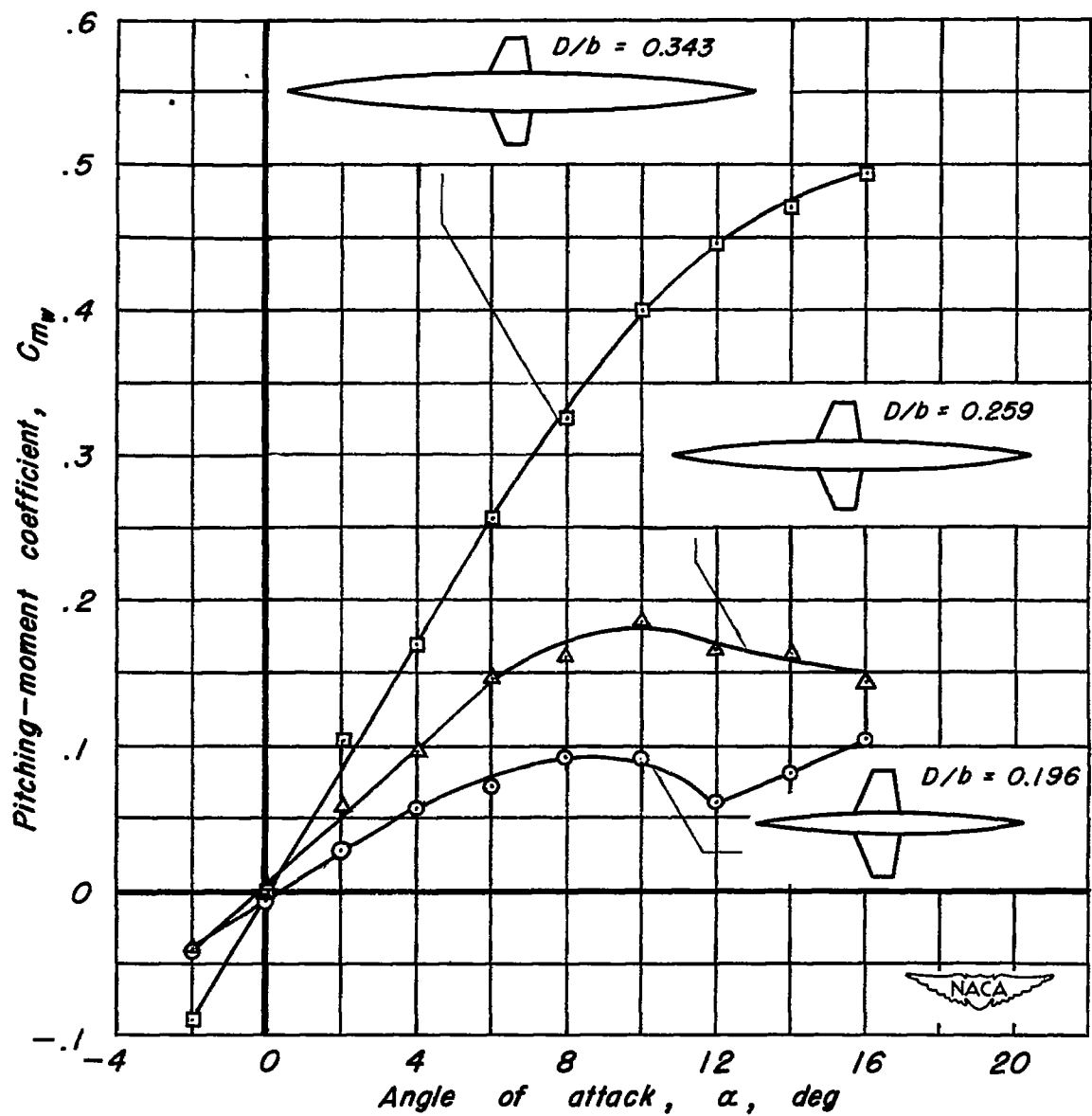
(c) C_{M_W} vs α

Figure 10.—Concluded.
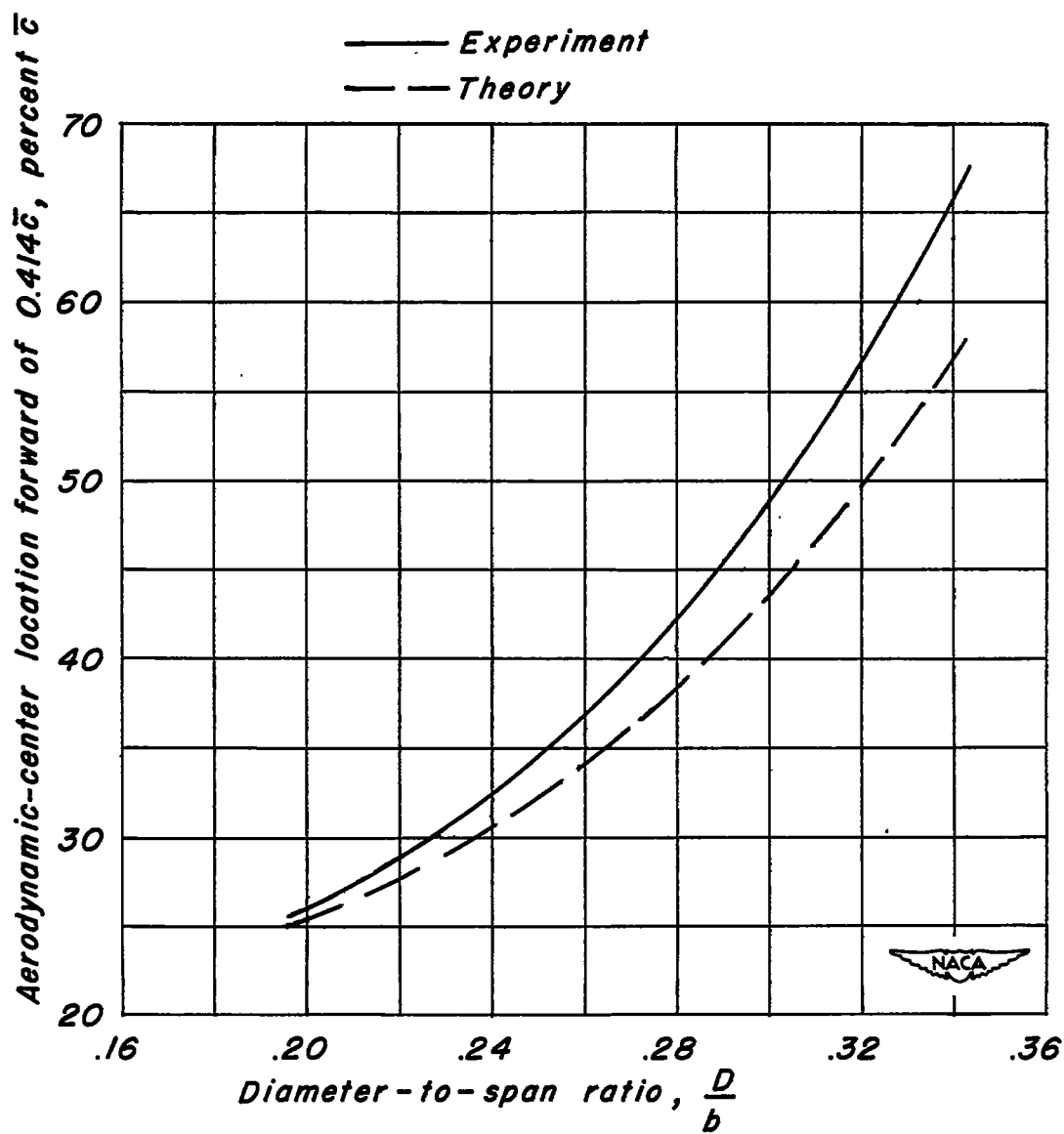
Figure 11.- Effect of body size on the aerodynamic-center locations for the wing-body combinations.
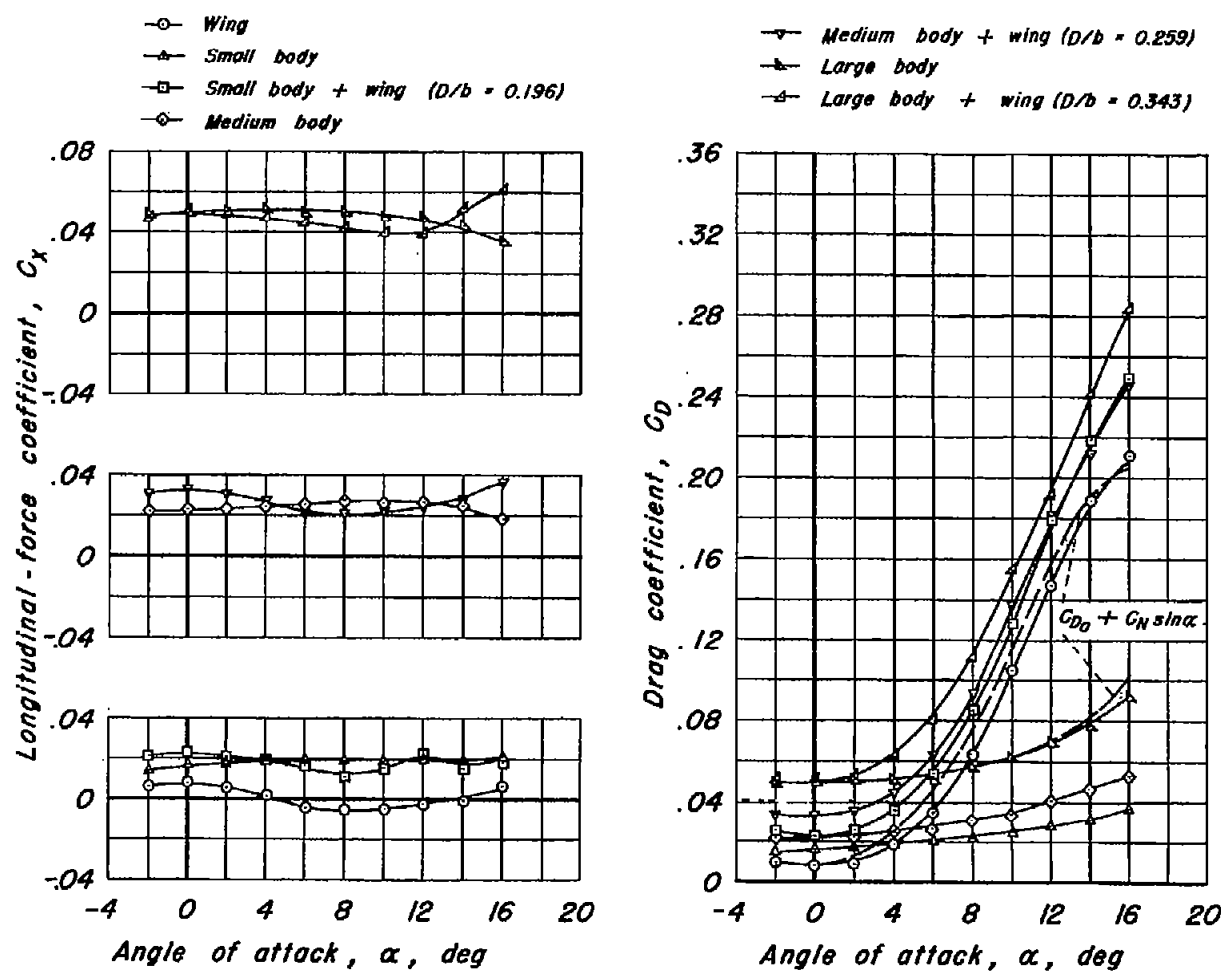
Figure 12.- Longitudinal-force and drag characteristics of the wing, the three bodies of revolution, and the three wing-body combinations.
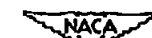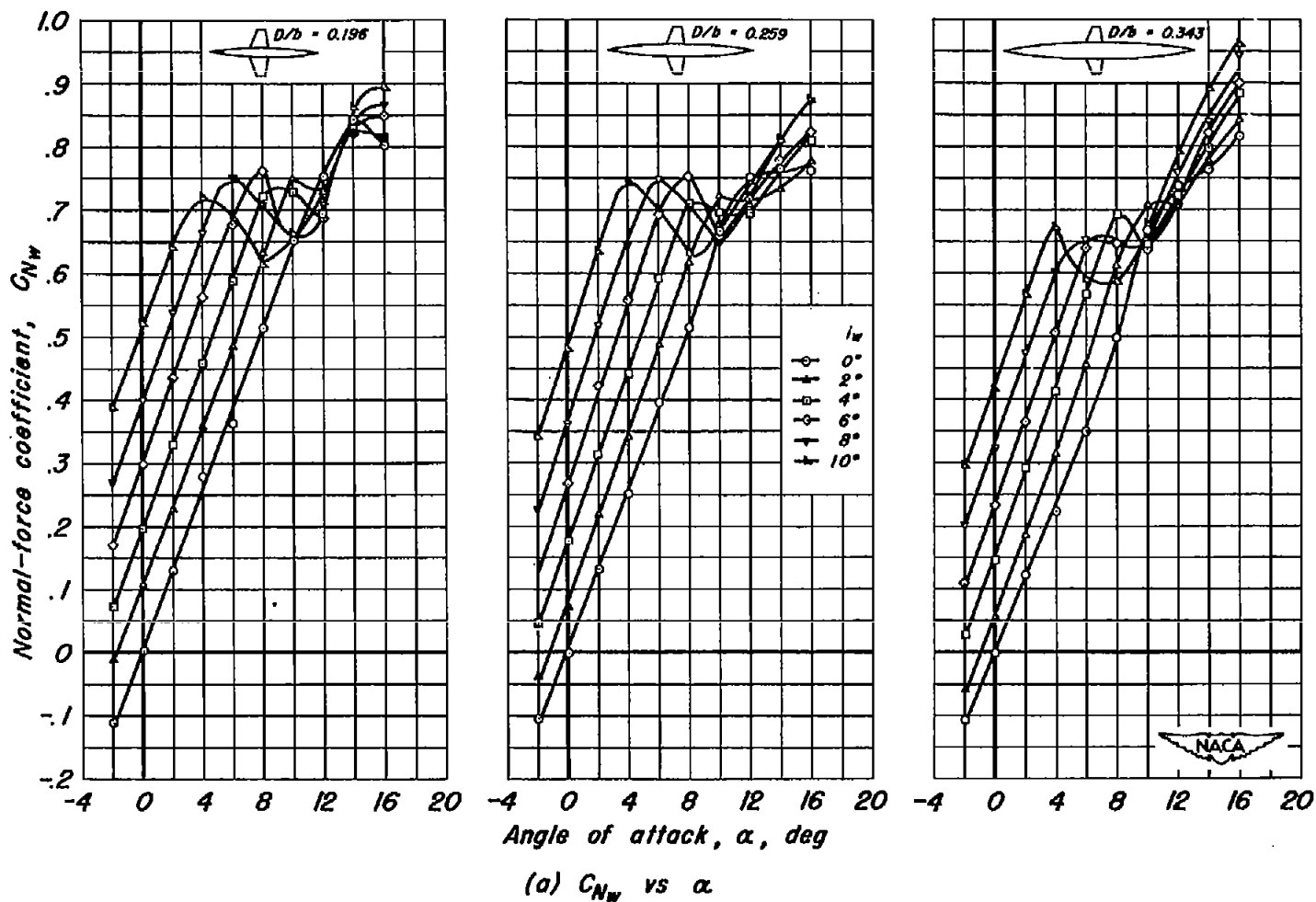
(a) C_{N_W} vs α

Figure 13.- Effect of change in the angle of wing incidence on the aerodynamic characteristics of the wing-body combinations.
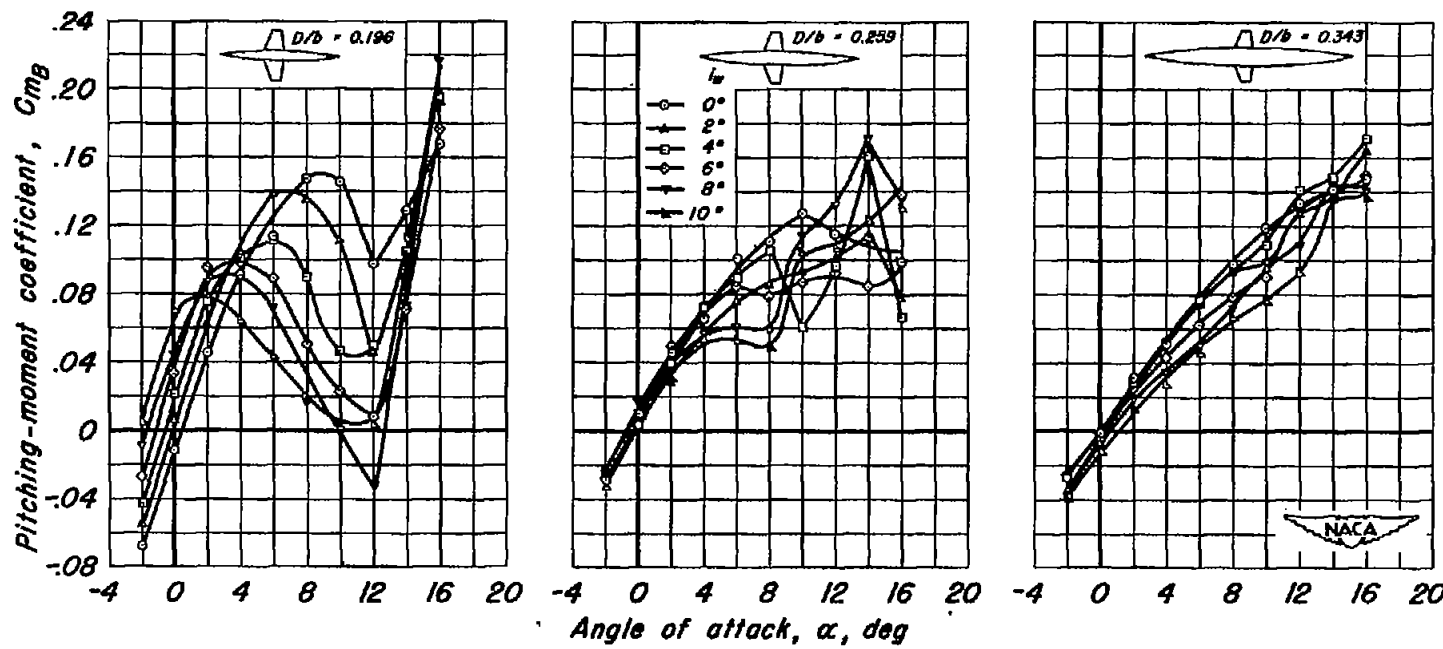
(b) C_{m_B} vs α

Figure 13.- Continued.
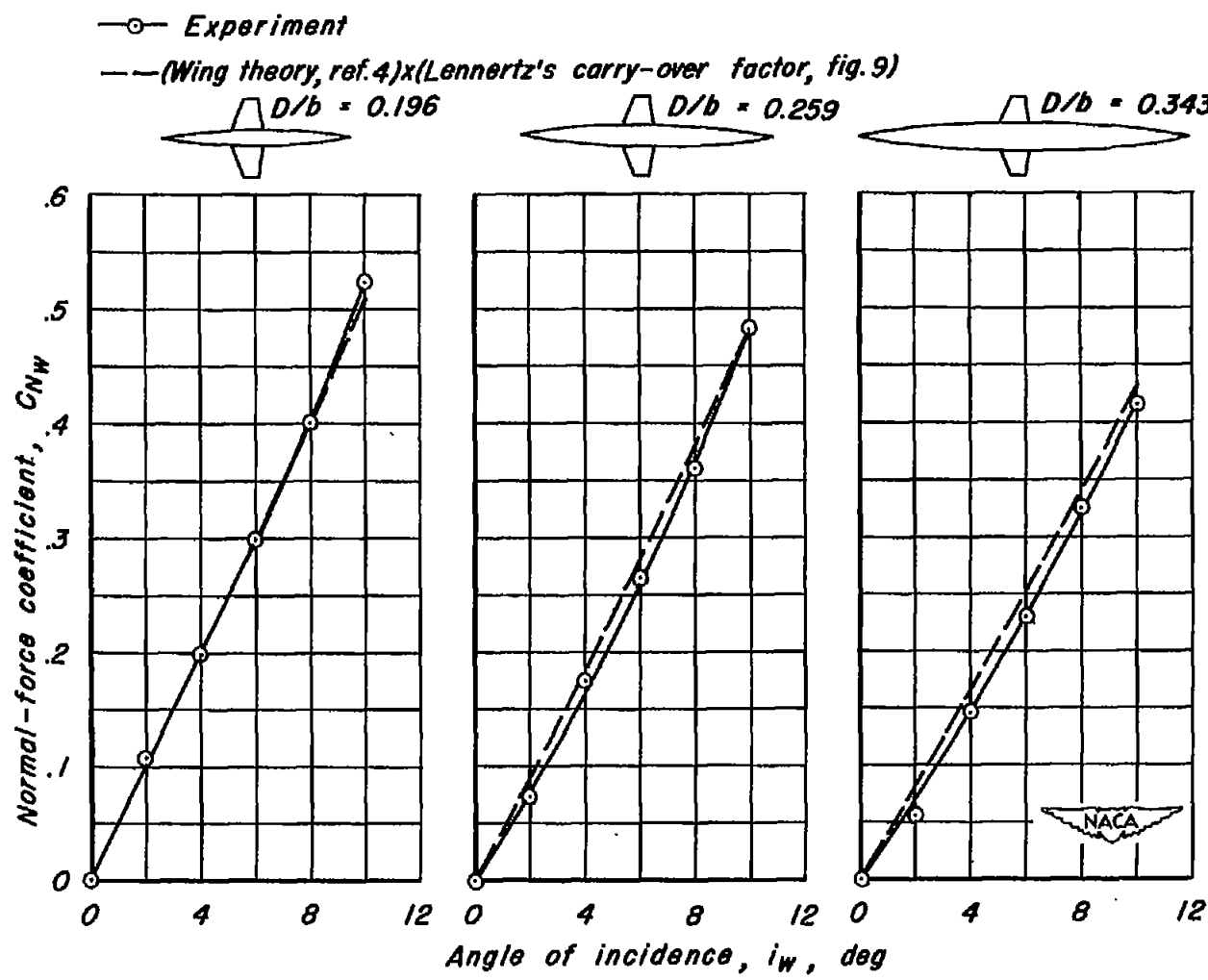
(c) C_{N_W} vs i_W $(\alpha = 0°)$

Figure 13.- Concluded.
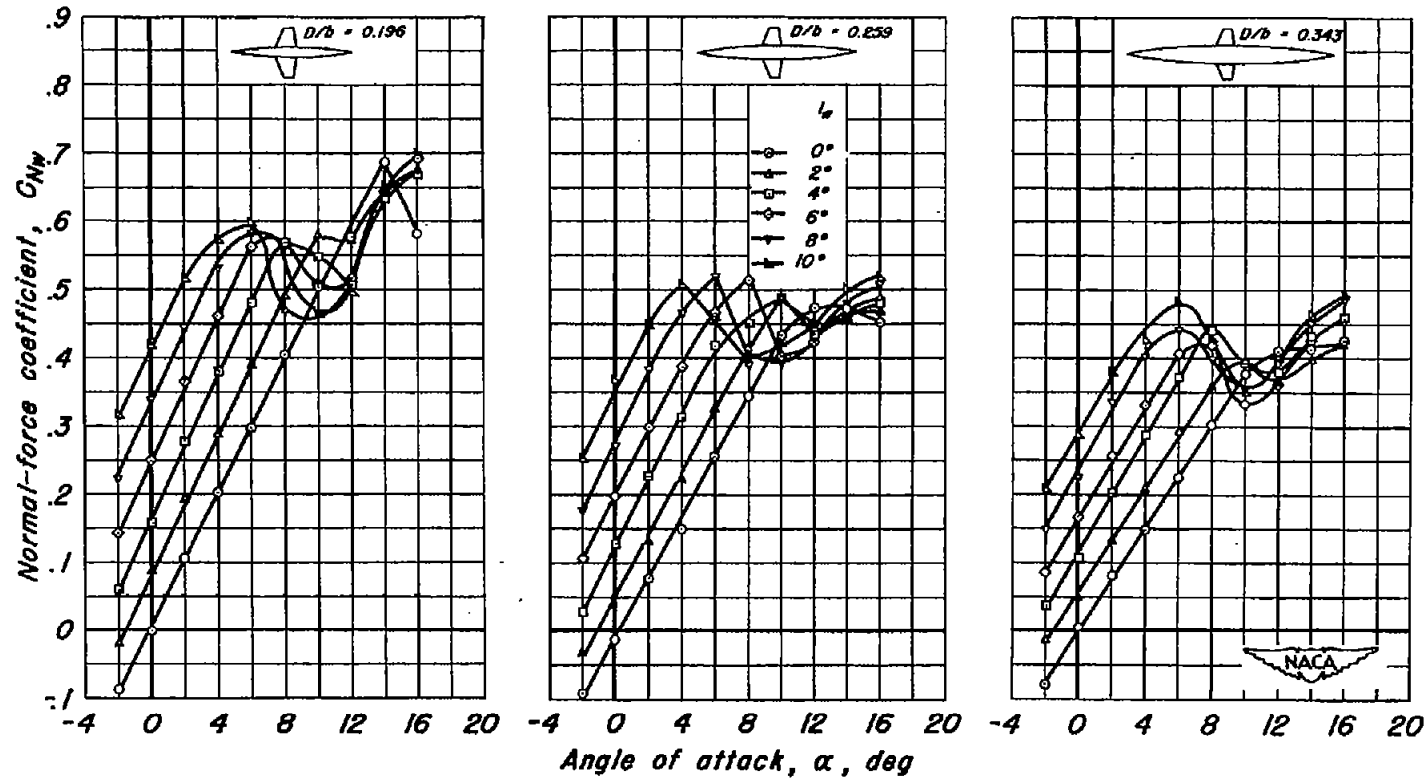
(a) C_{N_W} vs α

Figure 14.— Effect of change in the angle of wing incidence on the aerodynamic characteristics of the wing in the presence of the bodies of revolution.
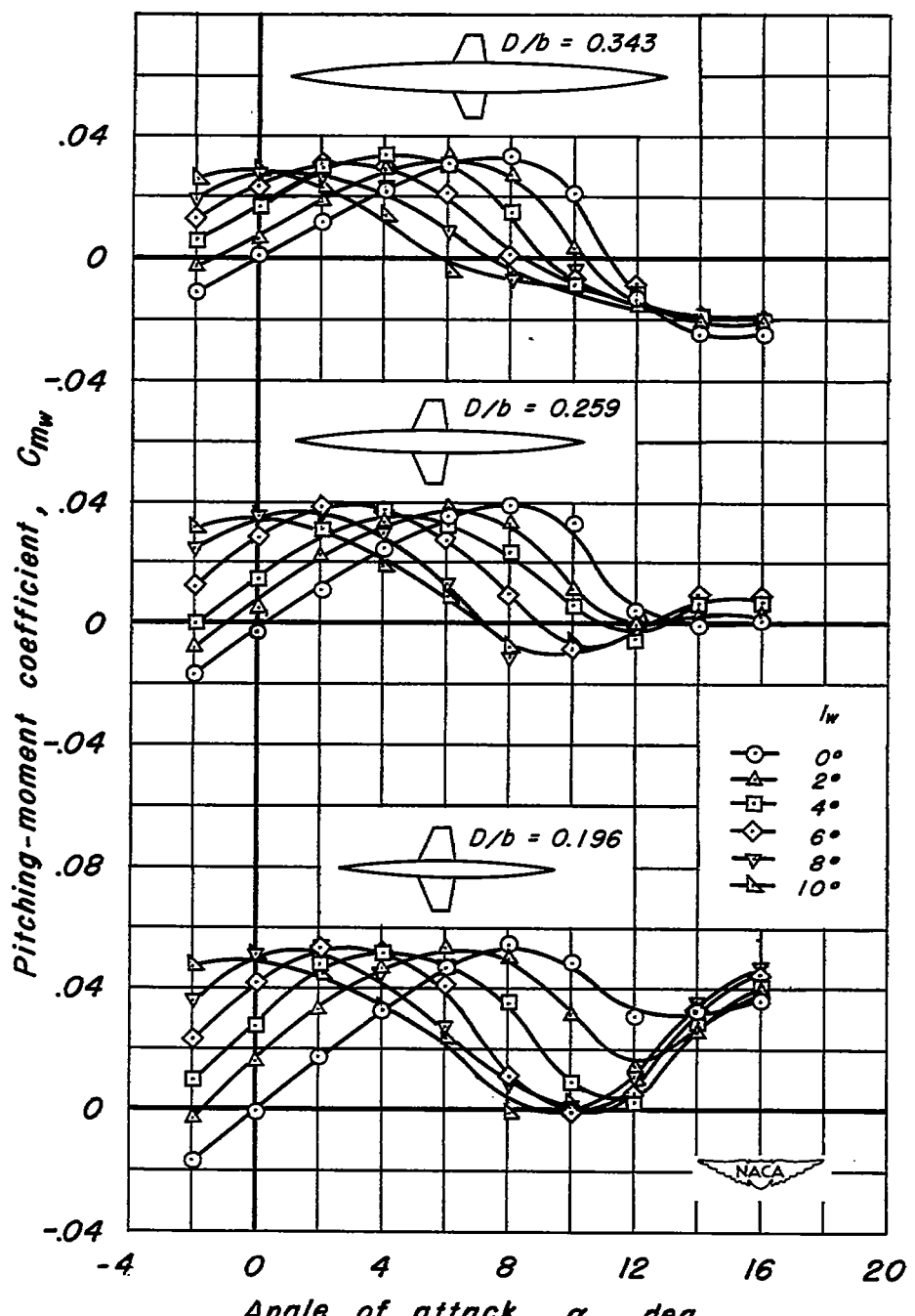
(b) C_{m_W} vs α

Figure 14.- Continued.
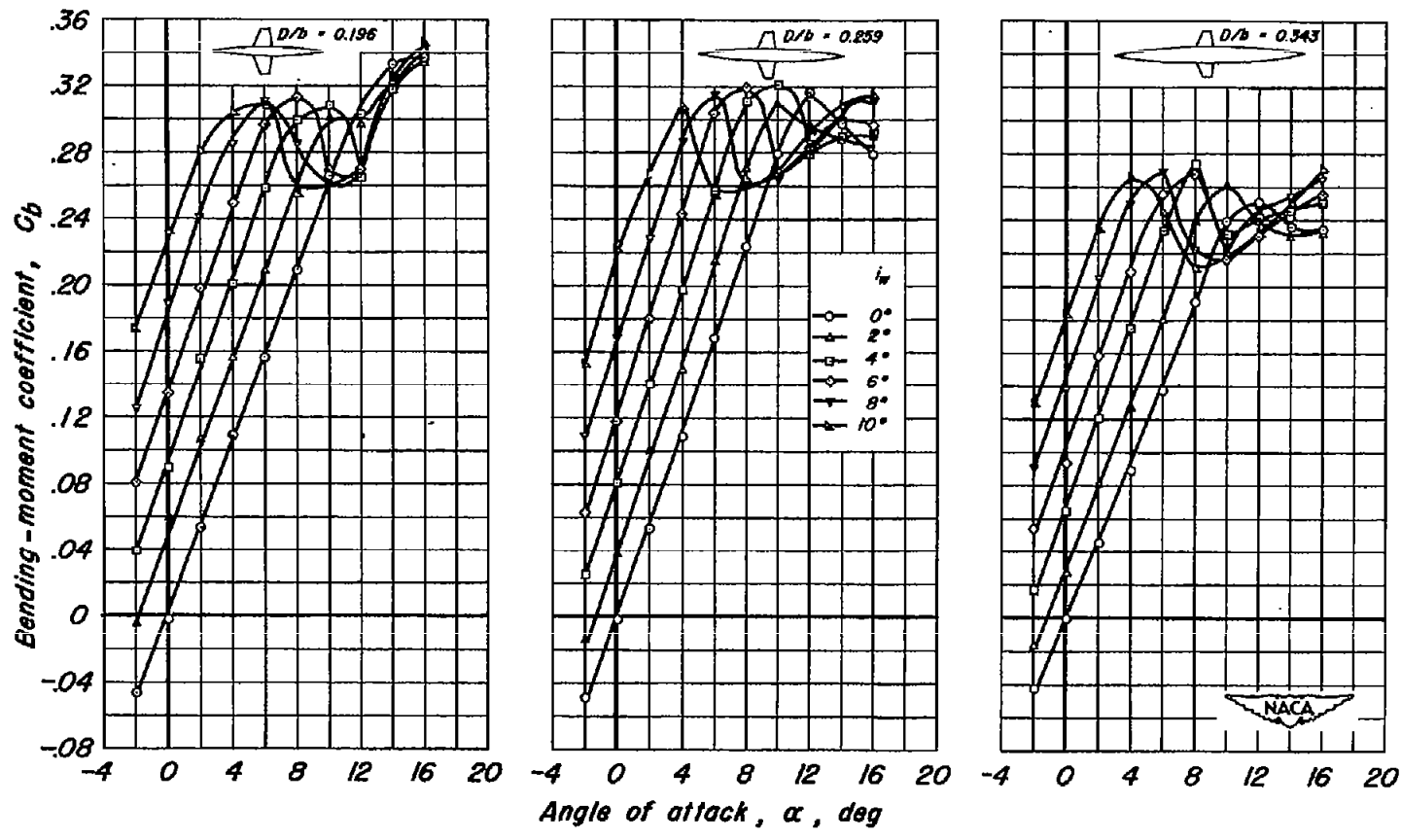
(c) C_b vs α

Figure 14.- Continued.
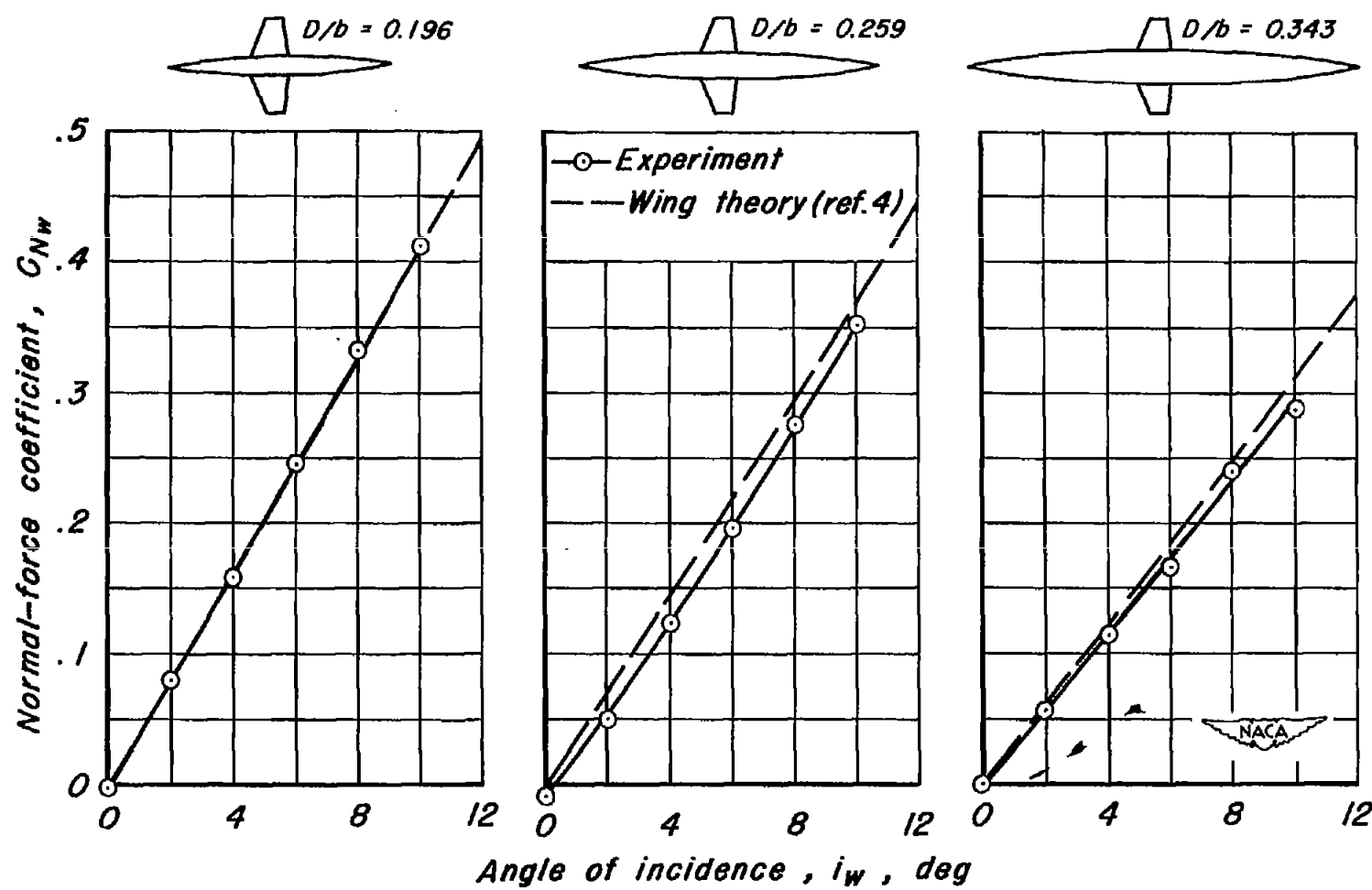
(d) C_{N_W} vs i_W ($\alpha = 0°$)

Figure 14.- Continued.

(s) C_b vs i_w $(\alpha = 0°)$

Figure 14.-   Concluded.